DMD Fast Forward. Published on August 11, 2015 as DOI: 10.1124/dmd.115.065656
This article has not been copyedited and formatted. The final version may differ from this version.

Title Page:

Defining human pathways of drug metabolism in vivo through the development of a multiple humanized mouse model

Nico Scheer, Yury Kapelyukh, Anja Rode, Stefan Oswald, Diana Busch, Lesley A. McLaughlin, De Lin, Colin. J. Henderson and C. Roland Wolf

Taconic Biosciences GmbH, Neurather Ring 1, 51063 Köln, Germany (N.S., A.R.); University Medicine of Greifswald, Center of Drug Absorption and Transport (C_DAT), Department of Clinical Pharmacology, Felix-Hausdorff-Str. 3, 17487 Greifswald, Germany (S.O., D.B); Medical Research Institute, Ninewells Hospital and Medical School, University of Dundee, Dundee DD1 9SY, United Kingdom (Y.K., L.A.M., D.L., C.H., C.R.W)

DMD Fast Forward. Published on August 11, 2015 as DOI: 10.1124/dmd.115.065656
This article has not been copyedited and formatted. The final version may differ from this version.

Running Title Page:

Drug metabolism pathways in multiple humanized mouse model

Corresponding Author:

Prof. Roland Wolf

E-mail: c.r.wolf@dundee.ac.uk

Level 9, Jacqui Wood Cancer Centre

Medical Research Institute

University of Dundee

Ninewells Hospital & Medical School

Dundee, DD1 9SY, UK

Tel: +44(0)1382 383134

Fax: +44(0)1382 386419

Number of text pages: 50

Number of tables: 1

Number of figures: 5

Number of references: 59

Number of words in the abstract: 150

Number of words in the introduction: 748

Number of words in the discussion: 1140

Nonstandard Abbreviations:

CYP, cytochrome P450; Cyp2d/2c/3a KO, Cytochrome P450 2d, 2c and 3a triple knockout mice; DDIs, drug-drug interactions; EMC, erythromycin; HLM, human liver microsomes; hPXR/CAR/CYP3A4/7, humanized mice for PXR, CAR and CYP3A4/7; hPXR/CAR/CYP3A4/7/2D6/2C9, humanized mice for PXR, CAR, CYP3A4/7, CYP2D6 and CYP2C9; IP, intra-peritoneal; K_I, enzyme-inhibitor complex dissociation constant; k_{inact}, rate constant of inactive enzyme formation; KTZ, ketoconazole; MDZ, midazolam; PB, phenobarbital; PO, oral administration; RIF, rifampicin; WT, wild type

DMD Fast Forward. Published on August 11, 2015 as DOI: 10.1124/dmd.115.065656
This article has not been copyedited and formatted. The final version may differ from this version.

Abstract

Variability in drug pharmacokinetics is a major factor in defining drug efficacy and side-effects; there remains an urgent need, particularly with the growing use of polypharmacy, to obtain more informative experimental data predicting clinical outcomes. Major species differences in multiplicity, substrate specificity and regulation of enzymes from the cytochrome P450-dependent mono-oxygenase system play a critical role in drug metabolism. To develop an in vivo model for predicting human responses to drugs we generated a mouse where 31 P450 genes from the Cyp2c, Cyp2d, and Cyp3a gene families were exchanged for their relevant human counterparts. The model has been improved through additional humanization for the nuclear receptors CAR and PXR that control the expression of key drug metabolizing enzymes and transporters. In this most complex humanized mouse model reported to date, the P450s function as predicted and we illustrate how these mice can be applied to predict drug-drug interactions in man.

DMD Fast Forward. Published on August 11, 2015 as DOI: 10.1124/dmd.115.065656
This article has not been copyedited and formatted. The final version may differ from this version.

Introduction

Cytochrome P450-dependent mono-oxygenases (CYPs) play a major role in the metabolism and disposition of most therapeutic drugs, with > 80% of currently used drugs metabolized by these enzymes (Guengerich, 2008; Williams et al., 2004). The P450 system comprises a number of multi-gene families with individual members exhibiting a distinct pattern of substrate specificity (Nelson et al., 2004), and provides an adaptive response where on exposure to drugs or environmental chemicals transcription factors are activated which increase the expression of specific cytochrome P450s and drug transporters resulting in increased rates of elimination (Omiecinski et al., 2011). Two transcription factors, the constitutive androgen receptor (CAR) and the pregnane X receptor (PXR) play a pivotal role in this process (Stanley et al., 2006). This regulatory network is complex; both CAR and PXR can be activated by the same compounds and can activate an overlapping spectrum of detoxication genes.

To define how drugs may be handled in man it is critical to obtain a detailed analysis of these pathways. A number of *in vitro* and *in vivo* approaches have been developed to predict how drugs interact with the human P450 system and the consequences for drug therapy, involving *in vitro* screens using recombinant P450 enzymes, hepatic microsomal fractions or isolated hepatocytes (Gebhardt et al., 2003) and *in vivo* pharmacokinetic studies in animals (Tang et al., 2007). These data are then extrapolated to the human situation using *in silico* algorithms (Rostami-Hodjegan, 2012; Tang et al., 2007).

Although valuable these models have a number of limitations, including the challenge in predicting complex clinical outcomes from reductionist *in vitro* results and profound species differences between the pathways of drug disposition. In mice, for example, there are 34 cytochrome P450s in the major gene families involved in drug metabolism, i.e. the *Cyp1a*, *Cyp2c*, *Cyp2d* and *Cyp3a* gene clusters, whereas in humans there are eight (Nelson et al., 2004). Interestingly three human enzymes - CYP2C9, CYP2D6 and CYP3A4 - account for

~75% of all reactions, with CYP3A4 being the single most important human P450 accounting for ~45% of Phase 1 drug metabolism (Guengerich, 2008). Differences in number of gene-duplication events during the past ~65 million years since the human and mouse genomes have diverged prohibit the assignments of orthologous genes between human and mouse and unsurprisingly the substrate specificity of proteins within gene families varies greatly across species (Martignoni et al., 2006). Furthermore, regulation of cytochrome P450s and indeed drug transporters by xenobiotics through the nuclear receptors can also differ markedly between species (Scheer and Wolf, 2013). This adds a further confounding factor in predicting *in vivo* drug pharmacokinetics in man, restricting the utility of animal models in the prediction of drug-drug interactions (DDIs), which can lead to loss of efficacy and/or enhanced drug toxicity.

To improve the utility and predictability of *in vivo* models of drug metabolism we and others have embarked on programmes to humanize mice for both P450s and the transcription factors which control their expression (Cheung and Gonzalez, 2008; Scheer and Wolf, 2013; Shen et al., 2011). These include humanized models for PXR (Lichti-Kaiser and Staudinger, 2008; Ma et al., 2007; Scheer et al., 2010; Scheer et al., 2008; Xie et al., 2000; Zhou et al., 2006), CAR (Scheer et al., 2008; Zhang et al., 2002), CYP3A4 (Cheung et al., 2006; Granvil et al., 2003; Hasegawa et al., 2011; Kazuki et al., 2013; van Herwaarden et al., 2005; van Herwaarden et al., 2007; Yu et al., 2005) and CYP2D6 (Corchero et al., 2001; Scheer et al., 2012b) and CYP2C9 (Scheer et al., 2012a). These models have provided valuable information on specific human drug responses in relation to pharmacokinetics, DDIs and toxicity. Multiple humanized mouse models for PXR/CAR (Scheer et al., 2008), CYP2D6/CYP3A4 (Felmlee et al., 2008), PXR/CYP3A4 (Ma et al., 2008) and PXR/CAR/CYP3A4 (Hasegawa et al., 2011) have been created. Encouragingly, the latter model allowed quantitative predictions of clinical PXR/CYP3A4-mediated DDIs (Hasegawa et al., 2011). One limitation of the models created to date is that the human and remaining mouse proteins can both contribute to

drug metabolism, as demonstrated by specific mouse Cyp2c enzymes being active in the metabolism of the CYP3A4 substrate midazolam (van Waterschoot et al., 2008). To minimize such problems, we report the creation of a mouse model in which mouse Pxr and Car, together with the Cyp2c Cyp2d and Cyp3a gene clusters, have been exchanged with human PXR, CAR, and the CYP2C9, CYP2D6 and CYP3A4/7 loci, respectively. This hPXR/CAR/CYP3A4/2D6/2C9 mouse represents the most complex humanized model for any purpose described to date and we demonstrate its functionality and utility in predicting pathways of drug metabolism and pharmacokinetics in man.

DMD Fast Forward. Published on August 11, 2015 as DOI: 10.1124/dmd.115.065656
This article has not been copyedited and formatted. The final version may differ from this version.

Materials and Methods

Animal husbandry

Mice were housed and maintained as described previously (Scheer et al., 2008). Mice were housed on sawdust in solid-bottom, polypropylene cages and provided with RM1 pelleted diet (Special Diet Services Ltd., Essex, UK) and drinking water *ad libitum* before and throughout the studies. The temperature was maintained within the range of 19 to 23°C and relative humidity within the range of 40 to 70%. A 12h light/dark cycle was maintained. hPXR/CAR/CYP3A4/7/2D6/2C9 mice were obtained from Taconic Biosciences GmbH (Cologne, Germany) and were used for studies at University of Dundee following at least 5 days of acclimatization. Other transgenic strains were obtained from Taconic Biosciences GmbH and bred at University of Dundee. C57BL/6 mice were used as wild type (WT) controls. All animal procedures were performed under a United Kingdom Home Office licence, and approved by the Ethical Review Committee, University of Dundee. Mice homozygous for all of the humanized genes were used for experimental studies.

The in vivo interaction of midazolam with ketoconazole was studied using 31-65 weeks old male hPXR/CAR/CYP3A4/7/2D6/2C9 mice. The effect of phenobarbital treatment on the Cyp2b expression in hPXR/CAR/CYP3A4/7/2D6/2C9 mice was investigated using 34-63 weeks old female animals. Wild type and complex humanised mice used in all other studies were 18-22 weeks old males.

Generation of hPXR/CAR/CYP3A4/7/2D6/2C9 mice

hPXR/CAR/CYP3A4/7/2D6/2C9 mice were generated from the previously described hPXR (Scheer et al., 2010), hCAR (Scheer et al., 2008), hCYP3A4/7 (Hasegawa et al., 2011), hCYP2D6 (Scheer et al., 2012b) and hCYP2C9 (Scheer et al., 2012a) mice by breeding. The *Cyp3a* locus in the hPXR/CAR/CYP3A4/7/2D6/2C9 model was further modified by the additional inactivation of mouse Cyp3a13, which was not deleted in the original hCYP3A4/7

model. This was achieved by deletion of a 4.3kb *BglII* fragment including exons 1 and 2 and the promoter region of *Cyp3a13* essentially as described previously (van Herwaarden et al., 2007). Successful inactivation was demonstrated by the loss of *Cyp3a13* mRNA expression in the liver and intestine of Cyp3a13$^{-/-}$ mice compared to WT controls (data not shown). hCYP3A4/7/Cyp3a13$^{-/-}$ mice were obtained by backcrossing hCYP3A4/7 and Cyp3a13$^{-/-}$ animals and selection of offspring with allelic crossover of both loci.

Rifampicin and phenobarbital treatment

In order to induce the expression of CYP3A4 mice were given three intra-peritoneal (IP) daily doses of rifampicin (RIF) (10 mg/kg) or vehicle control (corn oil) and euthanized 24 or 48h after the last dosing using a rising concentration of CO_2. In case of phenobarbital (PB), mice were given three daily doses of PB (80 mg/kg x2, then 40mg/kg, IP) or vehicle control (PBS) and euthanized 24 hours after the last treatment using a rising concentration of CO_2.

Collection of liver, duodenum, jejunum and ileum and preparation of microsomes

On the day of termination the mice were weighed, the body weights recorded, and then the mice transferred to a suitable room for post mortem. The mice were killed by exposure to a rising concentration of CO_2.

For liver collection and microsome preparation the gall bladder was removed, and then the liver was removed, weighed and scissor-minced in ice-cold KCl (1.15% w/v) for subsequent liver subcellular fractionation. The fresh liver samples were homogenized in ice-cold SET buffer (0.25 M sucrose, 5 mM EDTA, and 20 mM Tris-HCL, pH 7.4) to make a 10% (w/v) homogenate solution (9 ml SET buffer/1 g liver) using Polytron homogenizer. Microsomes were prepared by centrifugation first at 2000 rpm (Sorvall RTH-250 rotor) for 10 minutes at 4°C; then the supernatant was spun at 12000 rpm (Sorvall SS-34 rotor) for 20 minutes at 4°C. The resulting supernatant was centrifuged at 29130 rpm (Sorvall TFT-45.6 rotor) for 90

DMD Fast Forward. Published on August 11, 2015 as DOI: 10.1124/dmd.115.065656
This article has not been copyedited and formatted. The final version may differ from this version.

minutes at 4°C, and the microsomal pellets was resuspended in ice-cold SET buffer and stored at –70°C.

In case of intestinal collections and microsome preparation the small intestine was removed and flushed with ice cold phosphate buffered saline (PBS) containing a protease inhibitor cocktail (Roche Diagnostics, Basel, Switzerland). The duodenum, jejunum and ileum sections (approximately 10 cm each) was transferred into separate polypropylene tubes, flash frozen immediately in liquid nitrogen and stored at approximately –70^{o}C prior until used for microsome preparation. Frozen duodenum, jejunum and ileum were homogenized in 5.5 ml of SET buffer containing protease cocktail inhibitor (Roche) and PMSF (1 mM) using a Polytron homogenizer. Tissue homogenates were subjected to subcellular fractionation by differential centrifugation similar to that described for the preparation of liver microsomes. Microsomal fractions were stored at approximately -70^{o}C prior to analysis.

Western blotting

Detection of cytochromes P450 in microsomal fractions was carried out by SDS-PAGE and Western blotting.

CYP3A4: A rabbit whole serum (WB-3A4; Cat# 458234; BD-Gentest, Woburn, MA) was used to detect the human CYP3A4. 3 µg of microsomal protein were loaded per sample. The controls were liver microsomes from individual human donors with low (Donor# HH13; Cat# 452138; BD-Gentest, Woburn, MA) and high (Donor# HFC205; Cat# 452138; BD-Gentest, Woburn, MA) CYP3A4 activity, pooled human liver microsomes (Cat# 452117; BD-Gentest, Woburn, MA) and membrane preparations from bacteria expressing human CYP3A4 recombinant protein (Pritchard et al., 1997) (0.1 pmol).

Cyp2b: Cyp2b expression in liver microsomes (10 µg per sample) was visualised using rabbit polyclonal antibodies raised against rat CYP2B10 (Forrester et al., 1992). In house prepared

DMD Fast Forward. Published on August 11, 2015 as DOI: 10.1124/dmd.115.065656
This article has not been copyedited and formatted. The final version may differ from this version.

microsomes from naïve and PB treated (80 mg/kg; 3 daily doses; IP) WT mice were used as controls.

CYP2C9: Rabbit polyclonal antibodies against human CYP2C9 (Cat# Ab10317; Millipore, Temecula, CA) was used to detect human CYP2C9 in 10 μg of microsomal protein. Pooled human liver microsomes (10 μg; Cat# 452117; BD-Gentest, Woburn, MA), in house prepared microsomes from CYP2C9 humanized mice (10 μg) (Scheer et al., 2012a) and membrane preparations from bacteria expressing human CYP2C9 recombinant protein (Pritchard et al., 1997) (0.1 pmol) were used as controls.

CYP2D6: CYP2D6 in microsomes (10 μg per sample) was detected using a mouse monoclonal anti human CYP2D6 antibodies (MAB-2D6; Cat# 458246; BD-Gentest, Woburn, MA). The controls were liver microsomes from individual human donors with low (Donor# HG43; Cat# 452138; BD-Gentest, Woburn, MA) and high (Donor# HH37; Cat# 452138; BD-Gentest, Woburn, MA) CYP2D6 activity, pooled human liver microsomes (Cat# 452117; BD-Gentest, Woburn, MA) and membrane preparations from bacteria expressing human CYP2D6 (Pritchard et al., 1998) recombinant protein (0.05 pmol).

Enzyme activity measurements and in vitro inhibition studies

Midazolam 1'-hydroxylation: Midazolam (MDZ) (0.39-50 μM) was incubated with liver microsomes (0.05 mg protein/ml for RIF treated (termination 24h after the last RIF dose) hPXR/CAR/CYP3A4/7/2D6/2C9 microsomes and 0.25 mg protein/ml for all other microsomal preparations) and NADPH (1 mM) in 50 mM HEPES buffer (pH 7.4) supplemented with $MgCl_2$ (15 mM) and EDTA (0.1 mM) at 37°C. After 2 min, the reaction was stopped by adding to an equal volume of ice-cold acetonitrile, containing internal standard triazolam. Samples were centrifuged for 45 minutes at approximately 1,500xg on a Legend RT centrifuge (Sorvall, Newton, CT) and the concentration of 1'-hydroxymidazolam in the supernatant measured by HPLC-MS/MS. Chromatographic separation was performed

on a Luna C18(2) column (5 µm, 150 x 2.0 mm) (Phenomenex) using an injection volume of 10 µl and a run time of 16 minutes. The multiple reaction monitoring parameters for 1'-hydroxymidazolam and triazolam were 342.13, 343.08 (parent ion) and 203.05, 307.94 (collision ion), respectively. The concentrations of 1'- hydroxymidazolam were calculated from the calibration curve.

Inhibition of MDZ 1'-hydroxylation by ketoconazole: Ketoconazole (0.01-0.5 µM) was added to the incubation mixtures and the reactions were carried out essentially as described above, with the following exception. The protein concentration of liver microsomes from the RIF treated (termination 48h after the last rifampicin dose) hPXR/CAR/CYP3A4/7/2D6/2C9 mice was 0.25 mg protein/ml.

Inhibition of MDZ 1'-hydroxylation by erythromycin: For mechanism-based inhibition an erythromycin (0.152-3000 µM) microsome (final concentrations: 0.05 mg protein/ml for the RIF treated (termination 24h after the last RIF dose) hPXR/CAR/CYP3A4/7/2D6/2C9 microsomes and 0.25 mg protein/ml for all other microsomal preparations) mixture in 50 mM HEPES buffer (pH 7.4) supplemented with $MgCl_2$ (15 mM) and EDTA (0.1 mM) was incubated at 37°C in a water bath for 5 min prior to the reaction start by addition of NADPH regenerating system (final concentrations: 1 mM NADPH, 4 mM glucose-6-phosphate, 2 U/ml glucose-6-phosphate dehydrogenase). After 15 min MDZ was added (final concentrations were 3.1 µM, 4.46 µM and 4 µM for WT, human liver and hPXR/CAR/CYP3A4/7/2D6/2C9 microsomes, respectively) and the reaction was terminated 2 min later by adding to an equal volume of ice-cold acetonitrile, containing internal standard triazolam. Samples were centrifuged for 45 minutes at approximately 1,500xg on a Legend RT centrifuge (Sorvall, Newton, CT) and the concentration of 1'-hydroxymidazolam in the supernatant measured by HPLC-MS/MS as described in the section "Midazolam 1'-hydroxylation". The reversible inhibition experiment was performed as described above

except NADPH regenerating system was added after the 15 min incubation and subsequent addition of MDZ.

Inhibition of MDZ 1'-hydroxylation by CYP3cide: CYP3cide is a CYP3A4 specific time-dependent inhibitor (Walsky et al., 2012). Mixture of CYP3cide (0.5 and 5 μM), microsomes (0.8 mg protein/ml) and NADPH (1 mM) was incubated in 100 mM potassium phosphate buffer (pH 7.4) supplemented with $MgCl_2$ (3.3 mM) at 37°C for 320 s before transfer of the reaction aliquot (10 times final dilution) to MDZ (final concentration 50 μM) and NADPH (final concentration 1 mM) solution in the phosphate buffer. After 2 min of incubation at 37°C the MDZ hydroxylation was stopped by mixing with an equal volume of ice-cold acetonitrile, containing internal standard triazolam. No inhibitor controls were incubated with an equal volume of CYP3cide vehicle (ethanol). Positive controls contained ketoconazole (final concentration 10 μM) in the MDZ reaction solution. Samples were centrifuged for 45 minutes at approximately 1,500xg on a Legend RT centrifuge (Sorvall, Newton, CT) and the concentration of 1'-hydroxymidazolam in the supernatant measured by LC-MS/MS as it is described in the section "Midazolam 1'-hydroxylation".

Diclofenac 4'-hydroxylation: A diclofenac (4 μM) microsome (0.25 mg protein/ml) mixture with and without sulfaphenazole (50 μM) was incubated with NADPH (1 mM) in 100 mM potassium phosphate buffer (pH 7.4) supplemented with $MgCl_2$ (3.3 mM) at 37°C. After 5 min, the reaction was stopped by adding to an equal volume of ice-cold acetonitrile, containing internal standard bufuralol. Samples were centrifuged for 45 minutes at approximately 1,500xg on a Legend RT centrifuge (Sorvall, Newton, CT) and the concentration of 4'-hydroxydiclofenac in the supernatant determined by UPLC-MS/MS from the calibration curve. Compounds were separated on a Kinetex C18 column (1.7 μm, 50 x 2.1 mm) (Phenomenex) using an injection volume of 5 μl and a run time of 4 minutes. The multiple reaction monitoring parameters for 4'-hydroxydiclofenac and bufuralol were 312.15, 262.25 (parent ion) and 231.07, 188.13 (collision ion), respectively.

DMD Fast Forward. Published on August 11, 2015 as DOI: 10.1124/dmd.115.065656
This article has not been copyedited and formatted. The final version may differ from this version.

Bufuralol 1'-hydroxylation: A mixture of bufuralol (12.25 µM) and microsomes (0.25 mg protein/ml) with and without quinidine (5 µM) in 100 mM potassium phosphate buffer (pH 7.4) supplemented with $MgCl_2$ (3.3 mM) was incubated with NADPH (1 mM) at 37°C for 3 min before the reaction was stopped by mixing of the reaction mixture aliquot with equal volume of ice-cold acetonitrile containing triazolam as internal standard. Samples were centrifuged for 45 minutes at approximately 1,500xg on a Legend RT centrifuge (Sorvall, Newton, CT) and the concentration of 1'-hydroxybufuralol in the supernatant measured by UPLC-MS/MS. Chromatographic separation was performed on a Kinetex C18 column (1.7 µm, 50 x 2.1 mm) (Phenomenex) using an injection volume of 5 µl and a run time of 2 minutes. The multiple reaction monitoring parameters for 1'-hydroxybufuralol and triazolam were 278.43, 343.13 (parent ion) and 186.21, 308.10 (collision ion), respectively. Concentrations of the 1'-hydroxybufuralol in the samples were calculated from the calibration curve.

Pentoxyresorufin O-dependentylation: A mixture of pentoxyresorufin (5 µM) and microsomes (0.043-0.88 mg protein/ml) in 100 mM potassium phosphate buffer (pH 7.4) supplemented with $MgCl_2$ (3.3 mM) was incubated at 37°C for 5 min before the reaction was initiated by injection of NADPH (final concentration 1 mM). Generation of the fluorescent product was registered in a kinetic mode using Fluoroscan Ascent FL (Labsystems; excitation filter 530 nm; emission filter 585 nm). Slopes of the linear part of the kinetic curves were calculated using Ascent Software Version 2.4.1 (Labsystems). For each well with the reaction media there was a control well containing the reaction mixture with resorufin (4 pmol). Before addition of NADPH to the reaction wells, fluorescence was recorded both from the reaction and from the control wells. The average fluorescence was calculated and the difference between wells with and without resorufin was used for the conversion of the relative fluorescence units to the picomoles of the reaction product.

DMD Fast Forward. Published on August 11, 2015 as DOI: 10.1124/dmd.115.065656
This article has not been copyedited and formatted. The final version may differ from this version.

Absolute protein quantification of human CYP enzymes by LC-MC/MS

Absolute protein quantification of CYP2C9, CYP2D6 and CYP3A4 was carried out using microsomal fractions from intestinal and hepatic tissue by mass spectrometry-based targeted proteomics as recently described (Groer et al., 2014). GIFPLAER (CYP2C9), DIEVQGFR (CYP2D6) and EVTNFLR (CYP3A4) were used as validated protein specific surrogate peptides in parallel with their stable isotope-labelled internal standards. Accuracy (analytical error) and precision (coefficient of variation) of the assay during sample analysis were between ±15%, respectively. Final protein expression data (pmol/mg) were calculated by normalization to total protein content of the isolated microsomal fraction as determined by the bicinchoninic acid (BCA) assay (Pierce, Rockford, IL). In order to compare the protein abundance in the humanized model relative to levels in human, healthy human liver tissue (n=6, age: 34-68, gender: 3 males, 3 females) and jejunum (n=6, age: 51-73, gender: 2 males, 4 females) were analysed in parallel.

***In vivo* midazolam pharmacokinetics and DDI study**

Mice were divided in three groups (3 animals per group). Two groups were given three daily doses of RIF (10 mg/kg; 10 ml/kg; IP) and one group received vehicle (corn oil; 10 ml/kg; IP). One of the RIF-treated groups was administered ketoconazole (KTZ) (20 mg/kg in PEG400; 10 ml/kg; PO) 48 h after the last RIF dose and the two other groups were given vehicle (PEG400; 10ml/kg; PO). Midazolam (MDZ) (5 mg/kg in PEG400; 10 ml/kg; PO) was administered to all mice 30 min after the KTZ/vehicle dosing. Whole blood samples (10 µl) were collected at 10 min; 20 min; 40 min; 1h; 2h; 3h; 4h; 6h; 8h and 24 h after the administration of MDZ, placed immediately into microfuge tubes containing 10 µl heparin (15 U/ml) solution in MilliQ water, kept on ice and stored at approximately -20ºC prior to analysis. Concentrations of MDZ, 1'-hydroxymidazolam, 4-hydroxymidazolam and KTZ in whole blood were measured by LC/MS/MS. Calibration standards were prepared in whole

DMD Fast Forward. Published on August 11, 2015 as DOI: 10.1124/dmd.115.065656
This article has not been copyedited and formatted. The final version may differ from this version.

blood/water by adding an appropriate amount of corresponding analytical standards. The test samples and calibration standards (20 µl) were extracted in 65µl of acetonitrile containing triazolam (0.05 µg/ml) as internal standard, mixed on Thermomixer compact (Eppendorf) for approximately 5 min and centrifuged at approximately 16,100 g for 10 minutes. The supernatant was transferred to a 96-well plate and the concentrations of MDZ, 1'- hydroxy-midazolam, 4-hydroxy-midazolam and KTZ were measured by UPLC/MS/MS from the calibration curve. Chromatographic separation was performed on a Kinetex, C18 column (2.6 µm, 50 x 2.1 mm) (Phenomenex) using an injection volume of 30 µl and a run time of 6 minutes. The multiple reaction monitoring parameters for MDZ, 1'-hydroxy-midazolam, 4-hydroxy-midazolam, KTZ and triazolam were 326.08, 342.13, 342, 531.3, 343.08 (parent ion) and 291.01, 203.05, 234, 82, 307.94 (collision ion), respectively.

Data analysis for the inhibition of MDZ 1'-hydroxylation by KTZ

Data were analysed by simultaneous non-linear regression analysis (Kakkar et al., 1999; Kakkar et al., 2000) using GraFit 7.0.3 (Erithacus Software Limited, UK). For each microsomal preparation, complete data set (with and without KTZ) was fit simultaneously using mixed, non-competitive, competitive and uncompetitive inhibition models (**Scheme 1**; **Equation 1-4**).

MDZ and KTZ concentrations were two independent variables in the corresponding equations for the simultaneous non-linear regression.

$$v = \frac{V_{max} * [S]}{K_S * \left(1 + \frac{[I]}{K_i}\right) + [S] * \left(1 + \frac{[I]}{\alpha * K_i}\right)}$$

Equation 1 Mixed inhibition

$$v = \frac{V_{max} * [S]}{(K_S + [S]) * \left(1 + \frac{[I]}{K_i}\right)}$$

Equation 2 Non- competitive inhibition

$$v = \frac{V_{max} * [S]}{K_S * \left(1 + \frac{[I]}{K_i}\right) + [S]}$$

Equation 3 Competitive inhibition

DMD Fast Forward. Published on August 11, 2015 as DOI: 10.1124/dmd.115.065656
This article has not been copyedited and formatted. The final version may differ from this version.

$$v = \frac{V_{max} * [S]}{K_S + [S] * (1 + \frac{[I]}{K_i})}$$

Equation 4 Uncompetitive inhibition

Where v is a reaction rate; K_s is a dissociation constant of enzyme-substrate complex; K_i is a dissociation constant of enzyme-inhibitor complex; V_{max} is a reaction rate at infinite substrate concentration in the absence of inhibitor; α is a parameter describing the effect of inhibitor binding on the binding of substrate and vice versa; [S] and [I] are concentrations of the substrate and inhibitor, respectively.

For each microsomal preparation fits produced by different inhibition models were compared using QuickCalcs online application (GraphPad software, USA; http://graphpad.com/quickcalcs/aic1/). The preferable model between non-competitive, competitive and uncompetitive inhibition was selected by the lowest total sum of squares criteria. The selected model was subsequently compared to the mixed inhibition model by F test.

In liver microsomes from WT mice MDZ 1'-hydroxylation is catalysed not only by cytochromes P450 from the Cyp3a subfamily but also by mouse Cyp2c (Perloff et al., 2000). Mouse Cyp3a demonstrated notably higher affinity to KTZ compared to mouse Cyp2c (Perloff et al., 2000). Accordingly the kinetics of KTZ interaction with WT liver microsomes can be described in terms of inhibitor binding to two enzyme entities which have different affinities to the compound. Enzyme unit with relatively high affinity represents Cyp3a and that with the lower affinity reflects Cyp2c (**Scheme 2**).

Substrate and inhibitor binding to the individual Cyp3a component was studied in microsomes from Cyp2c knockout mice, where the Cyp2c contribution to MDZ 1'-hydroxylation was effectively eliminated. The inhibition was described by a non-competitive mechanism with the apparent dissociation constants of 2.6 μM and 0.013 μM for the enzyme complexes with MDZ and KTZ, respectively (**Supplementary Methods Table 1**; **Equation 5**). Similarly Cyp2c inhibition was investigated using Cyp3a knockout microsomes. The

DMD Fast Forward. Published on August 11, 2015 as DOI: 10.1124/dmd.115.065656
This article has not been copyedited and formatted. The final version may differ from this version.

inhibition mechanism was also non-competitive, however the dissociation constants for MDZ (8.6 μM) and KTZ (1.2 μM) were markedly higher compared to those from the Cyp2c knockout microsomes (**Supplementary Methods Table 1**; **Equation 6**)

$$v_{Cyp3a} = v_{Cyp2c\ KO} = \frac{V_{max(Cyp2c\ KO)} * [S]}{(K_{s\ (Cyp2c\ KO)} + [S]) * \left(1 + \frac{[I]}{K_{i\ (Cyp2c\ KO)}}\right)} = \frac{V_{max(Cyp2c\ KO)} * [S]}{(2.6 + [S]) * \left(1 + \frac{[I]}{0.035}\right)} \quad \textbf{Equation 5}$$

$$v_{Cyp2c} = v_{Cyp3a\ KO} = \frac{V_{max(Cyp3a\ KO)} * [S]}{(K_{s\ (Cyp3a\ KO)} + [S]) * \left(1 + \frac{[I]}{K_{i\ (Cyp3a\ KO)}}\right)} = \frac{V_{max(Cyp3a\ KO)} * [S]}{(8.6 + [S]) * \left(1 + \frac{[I]}{1.2}\right)} \quad \textbf{Equation 6}$$

Where v_{Cyp3a} ($v_{Cyp2c\ KO}$), and v_{Cyp2c} ($v_{Cyp3a\ KO}$) are the reaction rates catalysed by cytochrome P450s from the mouse Cyp3a and Cyp2c subfamily in microsomes from Cyp2c knockout and Cyp3a knockout mice, respectively; $V_{max(Cyp2c\ KO)}$ and $V_{max(Cyp3a\ KO)}$ are the reaction rates at infinite substrate concentration in the absence of inhibitor for Cyp2c knockout and Cyp3a knockout microsomes; $K_{s(Cyp2c\ KO)}$ and $K_{s(Cyp3a\ KO)}$ are enzyme-substrate complex dissociation constants for Cyp2c knockout and Cyp3a knockout microsomes; $K_{i(Cyp2c\ KO)}$ and $K_{i(Cyp3a\ KO)}$ are enzyme-inhibitor complex dissociation constants; [S] and [I] are substrate and inhibitor concentrations, respectively.

In WT microsomes both Cyp3a and Cyp2c are expressed. Thus the rate of MDZ 1'-hydroxylation can be presented as a sum of the reaction rates of Cyp3a and Cyp2c components. It is reasonable to assume that KTZ and MDZ interactions with each enzyme component in the WT microsomes have similar dissociation constants (K_i and K_s) to those measured for the individual enzyme subfamilies in the corresponding knockout microsomes. Therefore the dependency of the reaction rate in WT microsomes on the substrate and inhibitor concentrations can be expressed by **Equation 7** ("two-enzyme system"):

$$v_{Wild\ type} = v_{Cyp3a} + v_{Cyp2c} = \frac{V_{max(Cyp3a)} * [S]}{(2.6 + [S]) * (1 + \frac{[I]}{0.035})} + \frac{V_{max(Cyp2c)} * [S]}{(8.6 + [S]) * (1 + \frac{[I]}{1.2})} \quad \textbf{Equation 7}$$

Where $v_{Wild\ type}$ is the total reaction rate in WT microsomes; v_{Cyp3a} and v_{Cyp2c} are the reaction rates catalysed by Cyp3a and Cyp2c enzymes, respectively; $V_{max(Cyp3a)}$ and $V_{max(Cyp2c)}$ are the

DMD Fast Forward. Published on August 11, 2015 as DOI: 10.1124/dmd.115.065656
This article has not been copyedited and formatted. The final version may differ from this version.

reaction rates at infinite substrate concentration in the absence of inhibitor for Cyp3a and Cyp2c components; [S] and [I] are the corresponding substrate and inhibitor concentrations.

The concentrations of substrate and inhibitor in the equation are independent variables. $Vmax_{(Cyp3a)}$ and $Vmax_{(Cyp2c)}$ are parameters calculated by simultaneous non-linear regression of the inhibition data, which show the impact of the corresponding cytochrome P450 subfamily on the total reaction rate. Using similar considerations, MDZ 1'-hydroxylation in microsomes from hPXR/CAR/CYP3A4/7 mice can be presented as a general reaction catalysed by human CYP3A4 and mouse Cyp2c components. Values of MDZ and KTZ binding parameters for each of the components were calculated using inhibition data from human and Cyp3a knockout liver microsomes, respectively (**Supplementary Methods Table 1**; **Equation 1**; **Equation 6**). The corresponding reaction rate versus substrate and inhibitor concentration dependency is described by **Equation 8**.

$$v_{hPXR-hCAR-hCYP3A4/3A7} = v_{CYP3A4} + v_{Cyp2c} = \frac{Vmax_{(CYP3A4)}*[S]}{4.7*\left(1+\frac{[I]}{0.01}\right)+[S]*\left(1+\frac{[I]}{4.3*0.01}\right)} + \frac{Vmax_{(Cyp2c)}*[S]}{18.6+[S]*\left(1+\frac{[I]}{2.5}\right)} \qquad \textbf{Equation 8}$$

Where $v_{hPXR-hCAR-hCYP3A4/3A7}$ is the total reaction rate in liver microsomes from hPXR/CAR/CYP3A4/7 mice; v_{CYP3A4} and v_{Cyp2c} are reaction rates catalysed by CYP3A4 and Cyp2c enzymes, respectively; $V_{max(CYP3A4)}$ and $V_{max(Cyp2c)}$ are reaction rates at infinite substrate concentration in the absence of inhibitor for CYP3A4 and Cyp2c components; [S] and [I] are the corresponding substrate and inhibitor concentrations.

MDZ and KTZ binding parameters obtained during inhibition studies with human and mouse Cyp3a/Cyp2c/Cyp2d triple knockout microsomes described CYP3A4 and non-CYP3A4 components respectively in MDZ 1'-hydroxylation catalysed by microsomes from hPXR/CAR/CYP3A4/7/2D6/2C9 mice (**Equation 9**).

$$v_{Sextuple\ humanized} = v_{CYP3A4} + v_{Non-CYP3A4} = \frac{Vmax_{(CYP3A4)}*[S]}{4.7*\left(1+\frac{[I]}{0.01}\right)+[S]*\left(1+\frac{[I]}{4.3*0.01}\right)} + \frac{Vmax_{(Non-CYP3A4)}*[S]}{(43+[S])*\left(1+\frac{[I]}{0.6}\right)} \qquad \textbf{Equation 9}$$

Where $v_{Sextuple\ humanised}$ is the total reaction rate in liver microsomes from hPXR/CAR/CYP3A4/7/2D6/2C9 mice; v_{CYP3A4} and $v_{Non-CYP3A4}$ are reaction rates catalysed by

DMD Fast Forward. Published on August 11, 2015 as DOI: 10.1124/dmd.115.065656
This article has not been copyedited and formatted. The final version may differ from this version.

CYP3A4 and non-CYP3A4 enzymes, respectively; $V_{max(CYP3A4)}$ and $V_{max(Non\text{-}CYP3A4)}$ are reaction rates at infinite substrate concentration in the absence of inhibitor for CYP3A4 and non-CYP3A4 components; [S] and [I] are the corresponding substrate and inhibitor concentrations.

Inhibition data generated in WT, hPXR/CAR/CYP3A4/7 and hPXR/CAR/CYP3A4/7/2D6/2C9 mouse liver microsomes were fitted with the "two-enzyme" model. The goodness of fit for the "two-enzyme" and the most statistically preferable single enzyme model (mixed, non-competitive, uncompetitive or competitive) were compared using Akaike's method (**Supplementary Table 3**).

Time dependent inhibition of MDZ 1'-hydroxylation by EMC

Published method of time-dependent inhibition data analysis using IC_{50}-shift experimental setup (Berry and Zhao, 2008; Krippendorff et al., 2009; Maurer et al., 2000) was modified to allow simultaneous non-linear regression of the IC_{50} curves. It was assumed that substrate metabolism follows Michaelis-Menten kinetics with the rapid equilibrium approximation, inhibitor is competing with a substrate for the enzyme active site and the enzyme-inhibitor complex can produce inactive enzyme (**Scheme 3**).

The dependency of the reaction rate of substrate metabolism on substrate and inhibitor concentration can be described by **Equation 10**

$$v_i = \frac{k_{cat} * [E]_t * [S]}{K_m * \left(1 + \frac{[I]}{K_I}\right) + [S]} \qquad \textbf{Equation 10}$$

Where v_i is the reaction rate in the presence of inhibitor; k_{cat} is the turnover number; $[E]_t$ is the active enzyme concentration at time t; [S] is the substrate concentration; K_m is the Michaelis constant; [I] is the inhibitor concentration; K_I is the enzyme-inhibitor complex dissociation constant.

DMD Fast Forward. Published on August 11, 2015 as DOI: 10.1124/dmd.115.065656
This article has not been copyedited and formatted. The final version may differ from this version.

In the absence of inhibitor the reaction rate follows Michaelis-Menten kinetics and the active enzyme concentration $[E]_0$ remains unchanged during the course of the reaction (**Equation 11**).

$$v = \frac{k_{cat} * [E]_0 * [S]}{K_m + [S]} \qquad \textbf{Equation 11}$$

Where v is the reaction rate in the absence of inhibitor; $[E]_0$ is the active enzyme concentration.

The kinetics of enzyme inactivation in the presence of a mechanism-based inhibitor is described by **Equation 12** (Mayhew et al., 2000).

$$[E]_t = [E]_0 * e^{-\frac{k_{inact} * [I] * t}{K_I + [I]}} \qquad \textbf{Equation 12}$$

Where $[E]_t$ is the active enzyme concentration at time t; $[E]_0$ is the active enzyme concentration at time 0; k_{inact} is the rate constant of formation of inactive enzyme; [I] is the concentration of the mechanism-based inhibitor; t is time; K_I is the enzyme-inhibitor complex dissociation constant.

After substitution of the active enzyme concentration $[E]_t$ in **Equation 10**, **Equation 13** is obtained:

$$v_i = \frac{k_{cat} * [E]_0 * e^{-\frac{k_{inact} * [I] * t}{K_I + [I]}} * [S]}{K_m * \left(1 + \frac{[I]}{K_I}\right) + [S]} \qquad \textbf{Equation 13}$$

In IC_{50} curves the reaction rate is usually expressed as a percentage of that with no inhibitor. Therefore **Equation 13** can be divided by **Equation 11** and multiplied by 100% (**Equation 14**).

$$v_i(\%\ of\ v) = \frac{v_i}{v} * 100 = \frac{k_{cat} * [E]_0 * e^{-\frac{k_{inact} * [I] * t}{K_I + [I]}} * [S]}{K_m * \left(1 + \frac{[I]}{K_I}\right) + [S]} * \frac{K_m + [S]}{k_{cat} * [E]_0 * [S]} * 100 \qquad \textbf{Equation 14}$$

Where v_i(% of v) is the reaction rate expressed as a percentage of that with no inhibitor. After some simplifications **Equation 15** can be obtained:

DMD Fast Forward. Published on August 11, 2015 as DOI: 10.1124/dmd.115.065656
This article has not been copyedited and formatted. The final version may differ from this version.

$$v_i(\%\ of\ v) = \frac{e^{-\frac{k_{inact}*[I]*t}{K_I+[I]}}*(K_m+[s])}{K_m*\left(1+\frac{[I]}{K_I}\right)+[s]} * 100$$ **Equation 15**

If in the incubations substrate concentration was equal to K_m then further simplification of the **Equation 15** can be achieved (**Equation 16**).

$$v_i(\%\ of\ v) = \frac{e^{-\frac{k_{inact}*[I]*t}{K_I+[I]}}*200}{2+\frac{[I]}{K_I}}$$ **Equation 16**

The IC_{50} curves for inhibition of MDZ 1'-hydroxylation by EMC obtained with and without pre-incubation with the inhibitor were analysed by simultaneous non-linear regression analysis using **Equation 15** or **Equation 16** and software GraFit 7.0.3 (Erithacus Software Limited, UK). Inhibitor concentration and time were independent variables and k_{inact} and K_I were the calculated parameters.

DMD Fast Forward. Published on August 11, 2015 as DOI: 10.1124/dmd.115.065656
This article has not been copyedited and formatted. The final version may differ from this version.

Results

Generation and phenotypic analysis of hPXR/CAR/CYP3A4/7/2D6/2C9 mice

The generation of single hPXR (Scheer et al., 2010), hCAR (Scheer et al., 2008), hCYP3A4/7 (Hasegawa et al., 2011), hCYP2D6 (Scheer et al., 2012b) and hCYP2C9 (Scheer et al., 2012a) mice has been described previously. These mice have targeted replacement of mouse *Pxr* and *Car* with the corresponding human genes and the mouse *Cyp3a*, *Cyp2d* and *Cyp2c* gene clusters with human *CYP3A4*/*7*, *CYP2D6* and *CYP2C9* respectively. Human PXR and CAR in these models are known to be regulated by their corresponding mouse promoters; CYP3A4, CYP3A7 and CYP2D6 are known to be regulated by their cognate human promoters; and CYP2C9 is known to be regulated by the liver-specific mouse albumin promoter. Full genomic coding sequences of *CAR*, *CYP3A4*/*7* and *CYP2D6* are expressed in these models and hybrid human genomic/cDNA sequences of *PXR* and *CYP2C9*. The originally described hCYP3A4/7, hCYP2D6 and hCYP2C9 mice lack 14 of 15 *Cyp2c* genes (*Cyp2c29*, *Cyp2c37*, *Cyp2c38*, *Cyp2c39*, *Cyp2c40*, *Cyp2c50*, *Cyp2c54*, *Cyp2c55*, *Cyp2c65*, *Cyp2c66*, *Cyp2c67*, *Cyp2c68*, *Cyp2c69*, *Cyp2c70*), all nine *Cyp2d* genes (*Cyp2d9*, *Cyp2d10*, *Cyp2d11*, *Cyp2d12*, *Cyp2d13*, *Cyp2d22*, *Cyp2d26*, *Cyp2d34*, *Cyp2d40*) and seven of eight *Cyp3a* genes (*Cyp3a11*, *Cyp3a16*, *Cyp3a25*, *Cyp3a41*, *Cyp3a44*, *Cyp3a57*, *Cyp3a59*), respectively. The mouse *Cyp2c44* and *Cyp3a13* genes, which are both located at some distance from the main clusters, were not deleted in these models. In the new model we have additionally inactivated Cyp3a13 as described in the Materials and Methods section in order to eliminate a potential contribution of this P450 to drug pharmacokinetics. Cyp2c44, which has a low sequence homology with other mouse Cyp2c members, is not inducible by typical Cyp2c inducers and its role in drug metabolism is poorly defined (DeLozier et al., 2004), was not deleted. The individual humanizations included in the hPXR/CAR/CYP3A4/7/2D6/2C9 model are

summarized in **Fig. 1**. Homozygous hPXR/CAR/CYP3A4/7/2D6/2C9 mice were generated from the single humanized mice by breeding.

Basal and rifampicin-induced expression of CYP3A4, CYP2D6 and CYP2C9 protein in hPXR/CAR/CYP3A4/7/2D6/2C9 mice

Western blot analysis showed that the constitutive hepatic expression of CYP2D6 and CYP2C9 was comparable to the average expression measured in human liver (**Fig. 2a**). Treatment with RIF slightly reduced the expression of CYP2D6 and slightly increased the expression of CYP2C9. As previously observed in the single humanized mouse model the basal hepatic expression of CYP3A4 was low (Hasegawa et al., 2011), however, it was highly inducible following treatment with the human PXR activator, rifampicin (RIF). At the dose used (10mg/kg), hepatic CYP3A4 increased to levels equivalent to those found in human livers samples expressing high levels of this protein (**Fig. 2a**). The estimated concentration of CYP3A4 determined using a CYP3A4 standard curve, being 56 and 30 pmol/mg protein for the humanised mouse and the human liver sample respectively (data not shown).

CYP3A4 and CYP2D6 expression was detectable constitutively in the intestine. In both cases this was highest in duodenum, followed by jejunum and ileum (**Fig. 2b, c**). RIF treatment significantly increased the CYP3A4 levels in all regions of the intestine but had no effect on the expression of CYP2D6. As expected, CYP2C9, which is expressed under control of the liver-specific albumin promoter, was not detected in the intestine of the multiple humanized model. This was determined by LC-MS/MS (see below).

Quantification of hepatic and intestinal CYP3A4, CYP2D6 and CYP2C9 protein levels in hPXR/CAR/CYP3A4/7/2D6/2C9 mice by mass spectrometry

Protein levels of CYP3A4, CYP2D6 and CYP2C9 were further quantified by LC-MS/MS in liver, duodenum and jejunum samples from control and RIF-treated

hPXR/CAR/CYP3A4/7/2D6/2C9 mice (n=3 per group) and compared to the expression of these enzymes in human liver and jejunum (n=6 donors). It should be noted that the human liver samples used in this analysis were different to those used for the metabolism and Western blot studies. In agreement with the Western blot results, the expression of CYP3A4 in untreated mice was low but comparable with the expression level measured in the human donor with the lowest expression (1.3 pmol/mg protein) (**Supplementary Table 1**). Treatment of hPXR/CAR/CYP3A4/7/2D6/2C9 mice with RIF increased the hepatic CYP3A4 level to 220.7 ± 64.0 pmol/mg protein. This is approximately four fold higher than the level measured in a different set of samples by Western blot analysis (see above) but is within the range of that reported for human liver (Liu et al., 2014; Ohtsuki et al., 2012; Watanabe et al., 2004). Consistent with the Western blot data CYP3A4 was induced in the duodenum (from 2.8 ± 1.4 pmol/mg protein in control animals to 28.4 ± 18.3 pmol/mg protein in RIF treated mice), however because of the large variability in values between samples this change was not statistically significant. A comparison with human duodenum expression was not possible as no human samples were available. In the jejunum the constitutive level of CYP3A4 was similar to that found in human samples (3.6 ± 0.4 vs 2.1± 1.3 pmol/mg) but in this experiment was not increased on RIF treatment (3.1±1.4 nmol/mg) .

As anticipated, treatment with RIF did not significantly change hepatic or intestinal CYP2D6 levels in the hPXR/CAR/CYP3A4/7/2D6/2C9 mice (**Supplementary Fig. 1b**; **Supplementary Table 1**). Compared to the average expression in the human livers tested the CYP2D6 levels in these mice were ~4-fold higher in the liver (7.0±1.1 vs 27.2 ± 4.7 without and 28.3 ± 2.1 pmol/mg protein with RIF pretreatment) and 20-26-fold in the jejunum (0.2±1.1 vs 4.8 ± 5.6 without and 3.7 ± 3.2 pmol/mg protein with RIF pretreatment), respectively.

DMD Fast Forward. Published on August 11, 2015 as DOI: 10.1124/dmd.115.065656
This article has not been copyedited and formatted. The final version may differ from this version.

Hepatic CYP2C9 expression was significantly increased from 12.3 ± 2.1 to 23.6 ± 2.3 pmol/mg protein in the hPXR/CAR/CYP3A4/7/2D6/2C9 mice by RIF and both values were similar to the average expression of this enzyme in human liver (18.8 ± 5.2 pmol/mg protein) (**Supplementary Fig. 1c**; **Supplementary Table 1**). Consistent with the use of the liver-specific albumin promoter to drive the expression of CYP2C9 in the transgenic mice, no CYP2C9 protein was detectable in the duodenum and jejunum of these animals, compared to an average expression of 0.7 ± 0.3 pmol/mg protein in human jejunum.

Assessment of CAR, CYP3A4, CYP2D6 and CYP2C9 functional activity

Functional activity of PXR in the multiple humanized mouse model was demonstrated by the induction of CYP3A4 expression in response to treatment with the human PXR activator RIF (see above). In order to demonstrate functional CAR activity the hPXR/CAR/CYP3A4/7/2D6/2C9 mice were treated with the CAR activator phenobarbital (PB) and induction of Cyp2b10 protein and the Cyp2b-dependent pentoxyresorufin O-dealkylation determined. The expression of Cyp2b10 protein in hPXR/CAR/CYP3A4/7/2D6/2C9 mice was induced to a level similar to that in WT mice treated with PB (**Supplementary Fig. 2a**). The Cyp2b10 induction by PB was significantly more pronounced than the PXR-mediated increase of Cyp2b10 by RIF. An ~4-fold and ~30-fold increase in the metabolism of the Cyp2b10 substrate pentoxyresorufin in RIF and PB treated samples respectively paralleled the observed changes in protein expression (**Supplementary Fig. 2b**).

CYP3A4 activity was measured using the probe substrate midazolam (MDZ). Substrate dependencies for rates of MDZ 1'-hydroxylation were measured in corn oil WT, corn oil and RIF treated hPXR/CAR/CYP3A4/7/2D6/2C9 mouse, and pooled human liver microsomes (**Fig. 3a**; **Supplementary Table 2**). The V_{max} value of the microsomes from RIF-treated multiple humanized mice was approximately 3 and 10 times higher than that determined in

pooled human and WT mouse liver microsomes, respectively. Furthermore, RIF treatment increased the V_{max} of microsomes from hPXR/CAR/CYP3A4/7/2D6/2C9 mice by 58-fold compared to vehicle treated controls, while the K_m values were similar between the control and treated groups. The profound increase in MDZ 1'-hydroxylation in response to RIF is in agreement with the induction of CYP3A4 protein as determined by Western blot and protein quantification by LC-MS/MS (see above). These data demonstrate that CYP3A4 was functionally active in these mice. The similarity in K_m values along with the observation of low constitutive CYP3A4 background protein expression (**Fig. 2b; Supplementary Table 1**) suggests that MDZ 1'-hydroxylation in corn oil-treated hPXR/CAR/CYP3A4/7/2D6/2C9 mice is likely to be catalysed by constitutively expressed CYP3A4.

CYP2D6 activity was assessed by measuring metabolism of the probe substrate bufuralol. WT and hPXR/CAR/CYP3A4/7/2D6/2C9 liver microsomes showed a ~14 and 8-fold higher rate of bufuralol 1'-hydroxylation than pooled HLMs, respectively (**Fig. 3b**). The higher activity in the multiple humanized model can be partially explained by the 4-fold higher expression of CYP2D6 protein. The reaction was almost completely inhibited by the CYP2D6-specific inhibitor quinidine in human liver microsomal samples and samples from hPXR/CAR/CYP3A4/7/2D6/2C9 mice. This was not the case in samples from WT animals, demonstrating a marked species difference in the metabolism of this compound. Interestingly, bufuralol 1'-hydroxylation in microsomes from WT mice was ~11-fold higher than in microsomes from Cyp2d knockout mice(Scheer et al., 2012b), suggesting a major contribution from mouse Cyp2d enzymes. This difference increased to ~230 fold when comparing the activity in WT mice to that in microsomes from Cyp2c/Cyp2d/Cyp3a triple gene cluster knockout mice (Scheer et al., 2014), indicating the additional involvement of mouse Cyp2c and/or Cyp3a enzymes in this reaction.

CYP2C9 activity was assessed by measuring the metabolism of the CYP2C9 probe substrate diclofenac. In agreement with the Western blot (**Fig. 2a**) and protein quantification

(**Supplementary Fig. 1c**) data, diclofenac 4-hydroxylation in the liver microsomes from RIF-treated hPXR/CAR/CYP3A4/7/2D6/2C9 mice was approximately 1.5-fold higher compared to vehicle treated controls and ~90% of that measured in the pooled HLMs (**Fig. 3c**). In contrast, this activity was 4.6-fold lower in microsomes from WT animals compared to the vehicle-treated multiple humanized mice. Whilst the CYP2C9 specific inhibitor sulfaphenazole strongly decreased diclofenac 4-hydroxylation in human microsomes and microsomes from hPXR/CAR/CYP3A4/7/2D6/2C9 mice it had no effect in liver microsomes from WT mice. Also, there was no difference in the activity between microsomes from WT, Cyp2c KO and Cyp2c/Cyp2d/Cyp3a knockout mice suggesting that none of these enzyme subfamilies catalyse this reaction in mice. The contribution of other mouse enzymes to this activity explains the retention of some diclofenac 4-hydroxylation activity in microsomes from hPXR/CAR/CYP3A4/7/2D6/2C9 mice in the presence of sulfaphenazole.

The above data demonstrate the functional activity of CAR, CYP3A4, CYP2D6 and CYP2C9 in the multiple humanized mice.

Assessment of CYP3A4 contribution to 1'-hydroxylation of midazolam by microsomes from hPXR/CAR/CYP3A4/7/2D6/2C9 mice

A limitation of single CYP3A4 humanized mice is the significant contribution of mouse Cyp2c enzymes to the metabolism of substrates such as MDZ (van Waterschoot et al., 2008). This compromises the interpretation of any data obtained using this compound as a probe substrate in this model. The effect of the deletion of the *Cyp2c* gene cluster in the multiple humanized model on the metabolism of MDZ was investigated using liver microsomes from hPXR/CAR/CYP3A4/7/2D6/2C9 mice.

Whereas MDZ 1'-hydroxylation is catalysed by Cyp3a and Cyp2c enzymes in WT mice the Cyp3a component of this reaction is notably more sensitive to ketoconazole (KTZ) inhibition than the Cyp2c component (Perloff et al., 2000). We utilized this difference to delineate the

contribution of CYP3A4/Cyp3a enzymes to MDZ 1'-hydroxylation from that of Cyp2c/non-CYP3A4 proteins in liver microsomes from WT, and RIF-treated humanized PXR/CAR/CYP3A4/7 (hPXR/CAR/CYP3A4/7 (Hasegawa et al., 2011)) and hPXR/CAR/CYP3A4/7/2D6/2C9 mice. The data were analysed by developing a "two-enzyme" kinetic model to describe the relative affinities and contribution of each enzyme to MDZ metabolism (see Materials and Methods in the main text and Supplementary Methods for details). Inhibition of MDZ 1'-hydroxylation in microsomes from WT, hPXR/CAR/CYP3A4/7 and hPXR/CAR/CYP3A4/7/2D6/2C9 mice by KTZ was analysed by simultaneous non-linear regression using the "one enzyme" (mixed, non-competitive, competitive and uncompetitive) and corresponding "two-enzyme" inhibition models (**Equations 7-9** in Materials and Methods). The goodness of fit of the most statistically relevant "one enzyme" model was compared to that by the "two-enzyme" model (**Supplementary Table 3**; **Supplementary Fig. 3a-c**). Inhibition of MDZ 1'-hydroxylation by KTZ in WT and hPXR/CAR/CYP3A4/7 microsomes was significantly better described by the "two-enzyme" model than by the best fit "one-enzyme" model. This is consistent with the contribution of both Cyp3a and Cyp2c enzymes to this reaction in both sets of microsomes (**Supplementary Table 3**). The estimated contribution of hepatic Cyp2c in MDZ 1'-hydroxylation was ~35% for both mouse lines. In contrast, when the analysis was carried out using data derived from the hPXR/CAR/CYP3A4/7/2D6/2C9 samples the "one enzyme" system produced the best fit (**Supplementary Table 3**) providing evidence that all of the metabolism can be ascribed to CYP3A4. Statistically, the most preferable mode of inhibition was non-competitive with calculated dissociation constants for the enzyme-substrate and enzyme-inhibitor complex of 4.1 μM and 0.047 μM, respectively.

In order to confirm the above findings liver microsomes from WT, Cyp2c knockout, Cyp3a knockout, RIF-treated hPXR/CAR/CYP3A4/7 and hPXR/CAR/CYP3A4/7/2D6/2C9 mice were incubated with the potent and highly selective CYP3A4 time-dependent inhibitor,

DMD Fast Forward. Published on August 11, 2015 as DOI: 10.1124/dmd.115.065656
This article has not been copyedited and formatted. The final version may differ from this version.

CYP3cide,(Walsky et al., 2012) prior to assessing MDZ 1'-hydroxylation activity. Recombinant CYP3A4 co-expressed with cytochrome P450 reductase in bacterial membranes rather than HLMs was used, as HLM can contain CYP3A5 which also metabolises midazolam but is CYP3cide-insensitive. High concentrations of KTZ (10 μM) were used as a positive control in these studies. MDZ 1'-hydroxylation was not inhibited by CYP3cide in Cyp3a knockout microsomes but was decreased by 79% and 84% in Cyp2c knockout microsomes after incubation with 0.5 μM and 5μM inhibitor. These data suggest that mouse Cyp3a but not Cyp2c enzymes are sensitive to CYP3cide (**Fig. 4**). The activity of liver microsomes from RIF-treated hPXR/CAR/CYP3A4/7 mice was inhibited by 67% and 81% by 0.5μM and 5μM CYP3cide respectively. WT mouse liver microsomal fractions were more resistant to CYP3cide inhibition being inhibited with 52% and 61% respectively. This is consistent with the contribution of CYP3cide-insensitive mouse Cyp2c enzymes to MDZ 1'-hydroxylation. MDZ 1'-hydroxylation catalysed by recombinant CYP3A4 was inhibited by 78% and 91%, and that by microsomes from the hPXR/CAR/CYP3A4/7/2D6/2C9 mice by 93% and 96% at 0.5 μM and 5 μM CYP3cide, respectively. The latter finding provided evidence that enzymes other than CYP3A4 play only a very minor role in MDZ 1'-hydroxylation in this model.

In addition to KTZ and CYP3cide we tested the effect of the mechanism based inhibitor erythromycin (EMC) on CYP3A4 on MDZ 1'-hydroxylation. This inhibitor is metabolised to a product that forms an inhibitory complex with CYP3A4 (McConn et al., 2004). Therefore, in one experiment EMC, microsomes, MDZ and NADPH were incubated concomitantly, whilst in the other EMC was incubated with microsomes and cofactors for 15 min prior to the addition of MDZ (**Table 1 and Supplementary Fig. 4a-c**;). When incubated concomitantly an 18-fold lower IC_{50} was observed using HLM compared to WT mouse liver microsomes indicating a marked species difference in the affinity to EMC. The IC_{50} in microsomes from

DMD Fast Forward. Published on August 11, 2015 as DOI: 10.1124/dmd.115.065656
This article has not been copyedited and formatted. The final version may differ from this version.

hPXR/CAR/CYP3A4/7/2D6/2C9 mice was ~8-fold lower compared to that measured in WT microsomes but ~2-fold higher than that in pooled HLMs. The parameters for time dependent inhibition were obtained by simultaneous non-linear regression of the inhibition curves derived from experiments with and without pre-incubation with EMC as detailed in the Material and Methods. The estimated dissociation constant for the enzyme-inhibitor complex (K_I) was also 21-fold higher in WT samples compared to pooled HLMs which was only 3 fold lower than in microsomes from the multiple humanized mice. Calculated values for the rate constant of inactive enzyme formation (k_{inact}) were similar between WT and pooled HLMs, but 3-4-fold higher in hPXR/CAR/CYP3A4/7/2D6/2C9 microsomes. EMC inactivation efficiency (k_{inact}/K_I) was 16-fold higher in pooled HLMs compared to WT samples, mostly due to the higher compound affinity of the human enzyme. The inactivation efficiency in microsomes from the multiple humanized mice was comparable to HLMs and due to a combination of higher affinity to the inhibitor and a higher rate of inactivation, 21-fold higher compared to WT samples.

In vivo interactions of midazolam with rifampicin and ketoconazole in hPXR/CAR/CYP3A4/7/2D6/2C9 mice

Mice were treated IP with RIF (10mg/kg) or vehicle for 3 days followed by a single PO dose of MDZ 48 hours post RIF. One of the RIF-treated experimental groups was also given KTZ (PO) 30 min before MDZ administration. In the RIF-treated animals MDZ exposure decreased almost 8-fold (**Fig. 5a, b**) consistent with the observed strong induction of hepatic and, to a lesser degree, intestinal CYP3A4 (**Fig. 2b**; **Supplementary Fig. 1a**). On co-administration of KTZ a 1.9-fold increase in MDZ AUC was measured (**Fig. 5a, b**) indicative of inhibition of hepatic and/or intestinal CYP3A4. KTZ was rapidly eliminated and within 3 hours post MDZ the KTZ total blood concentration was decreased by 90% (**Fig. 5c**).

Discussion

The marked species differences between small mammals and man limits their utility in predicting drugs responses in humans. This includes predictions of pathways of drug disposition, bioavailability, drug efficacy, DDIs and toxicity. Although useful, current *in vitro* systems and *in silico* modelling approaches often have limitations in predicting the complex DDIs in different tissues under clinical conditions. In this paper we describe the generation and characterization of a novel sextuple humanized mouse model in which the major mouse gene families involved in drug metabolism have been deleted and exchanged for their human counterparts. The generation of this model has involved the replacement of 33 mouse genes with 6 human genes and represents the most complex model of multiple humanizations for any biochemical pathway described to date.

We demonstrate the functionality of this model system and how it can be used to predict drug pharmacokinetics in man. This versatile system can be used to investigate the relationship between drug exposure and efficacy, the capacity of drugs, at therapeutically relevant exposures, to alter their own metabolism or of drugs given in complex combinations to cause DDIs. In the era of polypharmacy this latter possibility addresses a current major area of clinical concern. An analysis of the use of prescribed drugs in Dundee, UK for example, has shown that more than 40% of individuals over the age of 70 are taking more than 8 drugs a day (2010 data; Medicines Monitoring Unit, http://www.dundee.ac.uk/memo/) demonstrating the enormous capacity for adverse drug reactions or loss of efficacy. Importantly, adverse drug reactions have been reported to be common causes of hospitalized death in the USA and in the UK (Lazarou et al., 1998; Pirmohamed et al., 2004). It is infeasible to evaluate all such DDIs by clinical trials and the model described in this paper can support the evaluation of drug combinations which may be of concern. Whilst possible DDI are reasons for concern in many areas of clinical practice, including treatment of cardiovascular and renal diseases, this is particularly important in oncology where most anti-cancer drugs are still used at close to the

DMD Fast Forward. Published on August 11, 2015 as DOI: 10.1124/dmd.115.065656
This article has not been copyedited and formatted. The final version may differ from this version.

maximum tolerated dose and changes in drug exposure can have life-threatening consequences.

The hPXR/CAR/CYP3A4/7/2D6/2C9 mice respond to drugs in a manner which more closely reflects the human situation both in terms of response to CAR and PXR activators and in relation to drug metabolism by key Phase 1 metabolising enzymes. When this model is used in conjunction with transgenic lines where specific nuclear receptors or P450 gene clusters have been deleted alone or in combination the ability to ascribe any results to a specific human P450 or signalling cascade is further increased (Scheer and Wolf, 2014). One significant advantage of the multiple relative to the single humanized mice stems from the significant functional redundancy in mouse cytochrome P450 gene families (van Waterschoot et al., 2008). This complicates the interpretation of experimental data as demonstrated in this work and by others in studies with MDZ, which is oxidised by P450s expressed by both the *Cyp2c* and *Cyp3a* gene families (van Waterschoot et al., 2008). These gene families have both been deleted in the multiple humanized model which circumvents this problem.

How the model overcomes species differences in drug inhibition is also reflected in the studies with the CYP2D6 and CYP2C9 substrates bufuralol and diclofenac. In WT mice these activities are not significantly inhibited by the CYP2D6 inhibitor quinidine and the CYP2C9 inhibitor sulfaphenazole (**Fig. 3b, c**) whereas in the humanized model they are. A similar situation was observed for CYP3A4-mediated MDZ 1'-hydroxylation by EMC (**Table 1; Supplementary Fig. 4**). These data further illustrate the utility of these animals to overcome the confounding impact of species differences in drug metabolism.

The human P450s in the model described, with the exception of CYP2C9, are regulated by their own promoters allowing the level of enzymes such as CYP3A4 to be varied in the liver and/or the gut by prior treatment of the mice with a P450 inducing agent. This facilitates studies not only to establish the role of the P450 system in defining drug oral bioavailability but also how variability in specific P450 levels will affect drug efficacy and/or side effects.

For example, we demonstrate that pre-treatment of the mice with RIF decreased the MDZ AUC ~8-fold (**Fig. 5a, b**). This is in good agreement with the results obtained from clinical studies (Backman et al., 1996). Also, the administration of KTZ to RIF-treated animals increased the MDZ AUC by 1.9-fold, somewhat lower than the ~5-fold change reported in humans, (Guest et al., 2011) and a possible explanation for this is as follows. At the time point of MDZ administration the whole blood concentration of KTZ was ~4 µg/ml; taking the binding of MDZ to erythrocytes into account this would translate to a plasma concentration of ~6 µg/ml, i.e. the plasma level reported in patients (Daneshmend et al., 1981). However, in patients this concentration reached a plateau at ~2h whereas in the humanized mice after 3 hours it declined by 90% of the initial concentration. Furthermore, the KTZ dose of 20 mg/kg in our study can be extrapolated to a dose of 113 mg/70 kg in man (Reagan-Shaw et al., 2008), lower than the 200 mg/kg KTZ dose used in the clinical studies which reported a 4.95-6.45 increase in MDZ AUC (Guest et al., 2011). Scaling the 1.9-fold MDZ AUC increase at a 113 mg equivalent KTZ dose in the multiple humanized mice to 200 mg would predict a ~3.4-fold increase in exposure. The human to mouse dose translation described above does not account for the rate of drug elimination (Reagan-Shaw et al., 2008). Considering the strong induction of CYP3A4 activity in the RIF-treated hPXR/CAR/CYP3A4/7/2D6/2C9 mice and relatively rapid elimination of the CYP3A4 substrate KTZ (Fitch et al., 2009) from the systemic circulation, the dose of the inhibitor in the induced hPXR/CAR/CYP3A4/7/2D6/2C9 mice has to be adjusted for the high activity of the major eliminating enzyme to adequately reflect the interaction of KTZ and MDZ in man. An empirical method of irinotecan dose calculation was developed to account for the inter-individual variations of activities of CYP3A4 in humans, which required collection of extensive *in vivo* experimental data (van der Bol et al., 2010). Applying a similar approach for dose translation between different species might be a more challenging task. Further dose adjustments of both RIF and KTZ may need to be made in future studies.

The hPXR/CAR/CYP3A4/7/2D6/2C9 mouse model described in this paper provides a powerful adjunct to existing experimental approaches for preclinical drug development and for optimizing drug use in patients. It offers the potential to study complex *in vivo* DDIs involving the enzyme system responsible for ~75% of the Phase 1 metabolism of all marketed drugs. In addition, it provides an excellent basis for further development, for example by introducing genetic modifications that reflect specific human diseases for predicting PK/PD relationships and it has significant potential application for the more informed design of clinical trials.

Acknowledgements

We wish to thank Julia Carr for technical assistance.

Authorship Contributions

Participated in research design: Scheer, Kapelyukh, Henderson, Oswald, Wolf

Conducted experiments: Kapelyukh, Rode, Busch, McLaughlin, Lin

Performed data analysis: Scheer, Kapelyukh, Oswald, Wolf

Wrote or contributed to the writing of the manuscript: Scheer, Kapelyukh, Henderson, Oswald, Wolf.

References

Backman JT, Olkkola KT and Neuvonen PJ (1996) Rifampin drastically reduces plasma concentrations and effects of oral midazolam. *Clin Pharmacol Ther* **59**(1): 7-13.

Berry LM and Zhao Z (2008) An examination of IC50 and IC50-shift experiments in assessing time-dependent inhibition of CYP3A4, CYP2D6 and CYP2C9 in human liver microsomes. *Drug Metab Lett* **2**(1): 51-59.

Cheung C and Gonzalez FJ (2008) Humanized mouse lines and their application for prediction of human drug metabolism and toxicological risk assessment. *J Pharmacol Exp Ther* **327**(2): 288-299.

Cheung C, Yu AM, Chen CS, Krausz KW, Byrd LG, Feigenbaum L, Edwards RJ, Waxman DJ and Gonzalez FJ (2006) Growth hormone determines sexual dimorphism of hepatic cytochrome P450 3A4 expression in transgenic mice. *J Pharmacol Exp Ther* **316**(3): 1328-1334.

Corchero J, Granvil CP, Akiyama TE, Hayhurst GP, Pimprale S, Feigenbaum L, Idle JR and Gonzalez FJ (2001) The CYP2D6 humanized mouse: effect of the human CYP2D6 transgene and HNF4alpha on the disposition of debrisoquine in the mouse. *Mol Pharmacol* **60**(6): 1260-1267.

Daneshmend TK, Warnock DW, Turner A and Roberts CJ (1981) Pharmacokinetics of ketoconazole in normal subjects. *J Antimicrob Chemother* **8**(4): 299-304.

DeLozier TC, Tsao CC, Coulter SJ, Foley J, Bradbury JA, Zeldin DC and Goldstein JA (2004) CYP2C44, a new murine CYP2C that metabolizes arachidonic acid to unique stereospecific products. *J Pharmacol Exp Ther* **310**(3): 845-854.

Felmlee MA, Lon HK, Gonzalez FJ and Yu AM (2008) Cytochrome P450 expression and regulation in CYP3A4/CYP2D6 double transgenic humanized mice. *Drug Metab Dispos* **36**(2): 435-441.

Fitch WL, Tran T, Young M, Liu L and Chen Y (2009) Revisiting the metabolism of ketoconazole using accurate mass. *Drug Metab Lett* **3**(3): 191-198.

Forrester LM, Henderson CJ, Glancey MJ, Back DJ, Park BK, Ball SE, Kitteringham NR, McLaren AW, Miles JS, Skett P and et al. (1992) Relative expression of cytochrome P450 isoenzymes in human liver and association with the metabolism of drugs and xenobiotics. *Biochem J* **281 (Pt 2)**: 359-368.

Gebhardt R, Hengstler JG, Muller D, Glockner R, Buenning P, Laube B, Schmelzer E, Ullrich M, Utesch D, Hewitt N, Ringel M, Hilz BR, Bader A, Langsch A, Koose T, Burger HJ, Maas J and Oesch F (2003) New hepatocyte in vitro systems for drug metabolism: metabolic capacity and recommendations for application in basic research and drug development, standard operation procedures. *Drug Metab Rev* **35**(2-3): 145-213.

Granvil CP, Yu AM, Elizondo G, Akiyama TE, Cheung C, Feigenbaum L, Krausz KW and Gonzalez FJ (2003) Expression of the human CYP3A4 gene in the small intestine of transgenic mice: in vitro metabolism and pharmacokinetics of midazolam. *Drug Metab Dispos* **31**(5): 548-558.

Groer C, Busch D, Patrzyk M, Beyer K, Busemann A, Heidecke CD, Drozdzik M, Siegmund W and Oswald S (2014) Absolute protein quantification of clinically relevant cytochrome P450 enzymes and UDP-glucuronosyltransferases by mass spectrometry-based targeted proteomics. *J Pharm Biomed Anal* **100**: 393-401.

Guengerich FP (2008) Cytochrome p450 and chemical toxicology. *Chem Res Toxicol* **21**(1): 70-83.

Guest EJ, Rowland-Yeo K, Rostami-Hodjegan A, Tucker GT, Houston JB and Galetin A (2011) Assessment of algorithms for predicting drug-drug interactions via inhibition mechanisms: comparison of dynamic and static models. *Br J Clin Pharmacol* **71**(1): 72-87.

Hasegawa M, Kapelyukh Y, Tahara H, Seibler J, Rode A, Krueger S, Lee DN, Wolf CR and Scheer N (2011) Quantitative prediction of human pregnane X receptor and cytochrome P450 3A4 mediated drug-drug interaction in a novel multiple humanized mouse line. *Mol Pharmacol* **80**(3): 518-528.

Kakkar T, Boxenbaum H and Mayersohn M (1999) Estimation of Ki in a competitive enzyme-inhibition model: comparisons among three methods of data analysis. *Drug Metab Dispos* **27**(6): 756-762.

Kakkar T, Pak Y and Mayersohn M (2000) Evaluation of a minimal experimental design for determination of enzyme kinetic parameters and inhibition mechanism. *J Pharmacol Exp Ther* **293**(3): 861-869.

Kazuki Y, Kobayashi K, Aueviriyavit S, Oshima T, Kuroiwa Y, Tsukazaki Y, Senda N, Kawakami H, Ohtsuki S, Abe S, Takiguchi M, Hoshiya H, Kajitani N, Takehara S, Kubo K, Terasaki T, Chiba K, Tomizuka K and Oshimura M (2013) Trans-chromosomic mice containing a human CYP3A cluster for prediction of xenobiotic metabolism in humans. *Hum Mol Genet* **22**(3): 578-592.

Krippendorff BF, Neuhaus R, Lienau P, Reichel A and Huisinga W (2009) Mechanism-based inhibition: deriving K(I) and k(inact) directly from time-dependent IC(50) values. *J Biomol Screen* **14**(8): 913-923.

Lazarou J, Pomeranz BH and Corey PN (1998) Incidence of adverse drug reactions in hospitalized patients: a meta-analysis of prospective studies. *JAMA* **279**(15): 1200-1205.

Lichti-Kaiser K and Staudinger JL (2008) The traditional Chinese herbal remedy tian xian activates pregnane X receptor and induces CYP3A gene expression in hepatocytes. *Drug Metab Dispos* **36**(8): 1538-1545.

Liu X, Hu L, Ge G, Yang B, Ning J, Sun S, Yang L, Pors K and Gu J (2014) Quantitative analysis of cytochrome P450 isoforms in human liver microsomes by the combination of proteomics and chemical probe-based assay. *Proteomics* **14**(16): 1943-1951.

Ma X, Cheung C, Krausz KW, Shah YM, Wang T, Idle JR and Gonzalez FJ (2008) A double transgenic mouse model expressing human pregnane X receptor and cytochrome P450 3A4. *Drug Metab Dispos* **36**(12): 2506-2512.

Ma X, Shah Y, Cheung C, Guo GL, Feigenbaum L, Krausz KW, Idle JR and Gonzalez FJ (2007) The PREgnane X receptor gene-humanized mouse: a model for investigating drug-drug interactions mediated by cytochromes P450 3A. *Drug Metab Dispos* **35**(2): 194-200.

Martignoni M, Groothuis GM and de Kanter R (2006) Species differences between mouse, rat, dog, monkey and human CYP-mediated drug metabolism, inhibition and induction. *Expert Opin Drug Metab Toxicol* **2**(6): 875-894.

Maurer TS, Tabrizi-Fard MA and Fung HL (2000) Impact of mechanism-based enzyme inactivation on inhibitor potency: implications for rational drug discovery. *J Pharm Sci* **89**(11): 1404-1414.

Mayhew BS, Jones DR and Hall SD (2000) An in vitro model for predicting in vivo inhibition of cytochrome P450 3A4 by metabolic intermediate complex formation. *Drug Metab Dispos* **28**(9): 1031-1037.

McConn DJ, 2nd, Lin YS, Allen K, Kunze KL and Thummel KE (2004) Differences in the inhibition of cytochromes P450 3A4 and 3A5 by metabolite-inhibitor complex-forming drugs. *Drug Metab Dispos* **32**(10): 1083-1091.

Nelson DR, Zeldin DC, Hoffman SM, Maltais LJ, Wain HM and Nebert DW (2004) Comparison of cytochrome P450 (CYP) genes from the mouse and human genomes, including nomenclature recommendations for genes, pseudogenes and alternative-splice variants. *Pharmacogenetics* **14**(1): 1-18.

Ohtsuki S, Schaefer O, Kawakami H, Inoue T, Liehner S, Saito A, Ishiguro N, Kishimoto W, Ludwig-Schwellinger E, Ebner T and Terasaki T (2012) Simultaneous absolute protein quantification of transporters, cytochromes P450, and UDP-glucuronosyltransferases as a novel approach for the characterization of individual human liver: comparison with mRNA levels and activities. *Drug Metab Dispos* **40**(1): 83-92.

Omiecinski CJ, Vanden Heuvel JP, Perdew GH and Peters JM (2011) Xenobiotic metabolism, disposition, and regulation by receptors: from biochemical phenomenon to predictors of major toxicities. *Toxicol Sci* **120 Suppl 1**: S49-75.

Perloff MD, von Moltke LL, Court MH, Kotegawa T, Shader RI and Greenblatt DJ (2000) Midazolam and triazolam biotransformation in mouse and human liver microsomes: relative contribution of CYP3A and CYP2C isoforms. *J Pharmacol Exp Ther* **292**(2): 618-628.

Pirmohamed M, James S, Meakin S, Green C, Scott AK, Walley TJ, Farrar K, Park BK and Breckenridge AM (2004) Adverse drug reactions as cause of admission to hospital: prospective analysis of 18 820 patients. *BMJ* **329**(7456): 15-19.

Pritchard MP, Glancey MJ, Blake JA, Gilham DE, Burchell B, Wolf CR and Friedberg T (1998) Functional co-expression of CYP2D6 and human NADPH-cytochrome P450 reductase in Escherichia coli. *Pharmacogenetics* **8**(1): 33-42.

Pritchard MP, Ossetian R, Li DN, Henderson CJ, Burchell B, Wolf CR and Friedberg T (1997) A general strategy for the expression of recombinant human cytochrome P450s in Escherichia coli using bacterial signal peptides: expression of CYP3A4, CYP2A6, and CYP2E1. *Arch Biochem Biophys* **345**(2): 342-354.

Reagan-Shaw S, Nihal M and Ahmad N (2008) Dose translation from animal to human studies revisited. *FASEB J* **22**(3): 659-661.

Rostami-Hodjegan A (2012) Physiologically based pharmacokinetics joined with in vitro-in vivo extrapolation of ADME: a marriage under the arch of systems pharmacology. *Clin Pharmacol Ther* **92**(1): 50-61.

Scheer N, Kapelyukh Y, Chatham L, Rode A, Buechel S and Wolf CR (2012a) Generation and characterization of novel cytochrome P450 Cyp2c gene cluster knockout and CYP2C9 humanized mouse lines. *Mol Pharmacol* **82**(6): 1022-1029.

Scheer N, Kapelyukh Y, McEwan J, Beuger V, Stanley LA, Rode A and Wolf CR (2012b) Modeling human cytochrome P450 2D6 metabolism and drug-drug interaction by a novel panel of knockout and humanized mouse lines. *Mol Pharmacol* **81**(1): 63-72.

Scheer N, McLaughlin LA, Rode A, Macleod AK, Henderson CJ and Wolf CR (2014) Deletion of 30 murine cytochrome p450 genes results in viable mice with compromised drug metabolism. *Drug Metab Dispos* **42**(6): 1022-1030.

Scheer N, Ross J, Kapelyukh Y, Rode A and Wolf CR (2010) In vivo responses of the human and murine pregnane X receptor to dexamethasone in mice. *Drug Metab Dispos* **38**(7): 1046-1053.

Scheer N, Ross J, Rode A, Zevnik B, Niehaves S, Faust N and Wolf CR (2008) A novel panel of mouse models to evaluate the role of human pregnane X receptor and constitutive androstane receptor in drug response. *J Clin Invest* **118**(9): 3228-3239.

Scheer N and Wolf CR (2013) Xenobiotic receptor humanized mice and their utility. *Drug Metab Rev* **45**(1): 110-121.

Scheer N and Wolf CR (2014) Genetically humanized mouse models of drug metabolizing enzymes and transporters and their applications. *Xenobiotica* **44**(2): 96-108.

Shen HW, Jiang XL, Gonzalez FJ and Yu AM (2011) Humanized transgenic mouse models for drug metabolism and pharmacokinetic research. *Curr Drug Metab* **12**(10): 997-1006.

Stanley LA, Horsburgh BC, Ross J, Scheer N and Wolf CR (2006) PXR and CAR: nuclear receptors which play a pivotal role in drug disposition and chemical toxicity. *Drug Metab Rev* **38**(3): 515-597.

Tang H, Hussain A, Leal M, Mayersohn M and Fluhler E (2007) Interspecies prediction of human drug clearance based on scaling data from one or two animal species. *Drug Metab Dispos* **35**(10): 1886-1893.

van der Bol JM, Mathijssen RH, Creemers GJ, Planting AS, Loos WJ, Wiemer EA, Friberg LE, Verweij J, Sparreboom A and de Jong FA (2010) A CYP3A4 phenotype-based dosing algorithm for individualized treatment of irinotecan. *Clin Cancer Res* **16**(2): 736-742.

van Herwaarden AE, Smit JW, Sparidans RW, Wagenaar E, van der Kruijssen CM, Schellens JH, Beijnen JH and Schinkel AH (2005) Midazolam and cyclosporin a metabolism in transgenic mice with liver-specific expression of human CYP3A4. *Drug Metab Dispos* **33**(7): 892-895.

van Herwaarden AE, Wagenaar E, van der Kruijssen CM, van Waterschoot RA, Smit JW, Song JY, van der Valk MA, van Tellingen O, van der Hoorn JW, Rosing H, Beijnen JH and Schinkel AH (2007) Knockout of cytochrome P450 3A yields new mouse models for understanding xenobiotic metabolism. *J Clin Invest* **117**(11): 3583-3592.

van Waterschoot RA, van Herwaarden AE, Lagas JS, Sparidans RW, Wagenaar E, van der Kruijssen CM, Goldstein JA, Zeldin DC, Beijnen JH and Schinkel AH (2008) Midazolam metabolism in cytochrome P450 3A knockout mice can be attributed to up-regulated CYP2C enzymes. *Mol Pharmacol* **73**(3): 1029-1036.

Walsky RL, Obach RS, Hyland R, Kang P, Zhou S, West M, Geoghegan KF, Helal CJ, Walker GS, Goosen TC and Zientek MA (2012) Selective mechanism-based inactivation of CYP3A4 by CYP3cide (PF-04981517) and its utility as an in vitro tool

for delineating the relative roles of CYP3A4 versus CYP3A5 in the metabolism of drugs. *Drug Metab Dispos* **40**(9): 1686-1697.

Watanabe M, Kumai T, Matsumoto N, Tanaka M, Suzuki S, Satoh T and Kobayashi S (2004) Expression of CYP3A4 mRNA is correlated with CYP3A4 protein level and metabolic activity in human liver. *J Pharmacol Sci* **94**(4): 459-462.

Williams JA, Hyland R, Jones BC, Smith DA, Hurst S, Goosen TC, Peterkin V, Koup JR and Ball SE (2004) Drug-drug interactions for UDP-glucuronosyltransferase substrates: a pharmacokinetic explanation for typically observed low exposure (AUCi/AUC) ratios. *Drug Metab Dispos* **32**(11): 1201-1208.

Xie W, Barwick JL, Downes M, Blumberg B, Simon CM, Nelson MC, Neuschwander-Tetri BA, Brunt EM, Guzelian PS and Evans RM (2000) Humanized xenobiotic response in mice expressing nuclear receptor SXR. *Nature* **406**(6794): 435-439.

Yu AM, Fukamachi K, Krausz KW, Cheung C and Gonzalez FJ (2005) Potential role for human cytochrome P450 3A4 in estradiol homeostasis. *Endocrinology* **146**(7): 2911-2919.

Zhang J, Huang W, Chua SS, Wei P and Moore DD (2002) Modulation of acetaminophen-induced hepatotoxicity by the xenobiotic receptor CAR. *Science* **298**(5592): 422-424.

Zhou J, Zhai Y, Mu Y, Gong H, Uppal H, Toma D, Ren S, Evans RM and Xie W (2006) A novel pregnane X receptor-mediated and sterol regulatory element-binding protein-independent lipogenic pathway. *J Biol Chem* **281**(21): 15013-15020.

Footnotes

This work was supported in part by a CRUK programme grant [C4639/A10822] awarded to CRW and by InnoProfile-Transfer grant [Grant-Nr. 03IPT612X] awarded to SO. Part of this work was supported by ITI Life Sciences, Scotland

N.S. current affiliation: Independent consultants, Cologne, Germany

N.S. and Y.K. contributed equally to this work

Scheme Legends

Scheme 1 Mixed (A), non-competitive (B), competitive (C) and uncompetitive (D) inhibition models used in the data analysis of inhibition of MDZ 1'-hydroxylation by KTZ

Scheme 2 "Two-enzyme" inhibition model used in the data analysis of inhibition of MDZ 1'-hydroxylation by KTZ

Scheme 3 Model of time-dependent enzyme inactivation in the presence of a substrate; under the rapid equilibrium approximation Ks≈Km

DMD Fast Forward. Published on August 11, 2015 as DOI: 10.1124/dmd.115.065656
This article has not been copyedited and formatted. The final version may differ from this version.

Figure Legends

Figure 1 Schematic overview of the individual humanizations included in the hPXR/CAR/CYP3A4/7/2D6/2C9 model. The intron/exon structure is shown for *PXR* and *CAR* with mouse exons indicated in black and with small type, human exons in grey and with capitals. The striped boxes represent poly-adenylation motifs included in the targeting vectors. The structure of the gene clusters is illustrated in case of *CYP3A*, *CYP2D* and *CYP2C* and genomic distances are indicated as kilobases (kb) or megabases (mb). Mouse genes and the direction of their transcription are shown as black arrows, human genes as grey boxes. Promoters driving the expression of the human genes are represented as white boxes. Dotted lines indicate the sites of replacement of mouse with human sequences. For the sake of clarity sequences are not drawn to scale.

Figure 2 Basal and inducible expression of CYP3A4, CYP2D6 and CYP2C9 in hPXR/CAR/CYP3A4/7/2D6/2C9 mice. (**a**) Expression of CYP3A4, CYP2D6 and CYP2C9 protein in liver microsomes from WT mice (n=3), corn oil-treated hPXR/CAR/CYP3A4/7/2D6/2C9 mice (n=2), RIF-treated hPXR/CAR/CYP3A4/7/2D6/2C9 mice (n=2) and human donors (HLM) determined by Western blot analysis using human specific antibodies (Ab). Donor 1 and donor 2 represent human individuals with low and high activity for CYP3A4 and CYP2D6, respectively. Donors with low and high activity for CYP2C9 were not available for this study and were therefore not tested. (**b**) CYP3A4 and (**c**) CYP2D6 protein expression in pooled liver, duodenum, jejunum and ileum microsomes from corn oil and RIF-treated hPXR/CAR/CYP3A4/7/2D6/2C9 mice (n =2 mice per treatment) determined by Western blot analysis. Controls (Contr.) are recombinant CYP3A4 or CYP2D6 and pooled HLM.

Figure 3 Functional activity of CYP3A4, CYP2D6 and CYP2C9 in hPXR/CAR/CYP3A4/7/2D6/2C9 mice. (**a**) Substrate concentration dependency for midazolam 1'-hydroxylation in microsomes from WT and hPXR/CAR/CYP3A4/7/2D6/2C9 mice and human donors. Formation of 1'-hydroxy-midazolam was measured in pooled liver microsomes from WT mice (n=3), a pool of human donors and corn oil- and RIF-treated hPXR/CAR/CYP3A4/7/2D6/2C9 mice (n=2 per treatment). All measurements were performed in duplicates; symbols represent individual data; lines are non-linear regression using Michaelis-Menten kinetic model. (**b**) Bufuralol 1'-hydroxylation and (**c**) diclofenac 4-hydroxylation in liver microsomes from WT, hPXR/CAR/CYP3A4/7/2D6/2C9, Cyp2d or Cyp2c knockout and Cyp2c/Cyp2d/Cyp3a knockout mice and human donors and inhibition of these reactions by quinidine (**b**) and sulfaphenazole (**c**). Data are expressed as mean ± SD (n=3 for WT, Cyp2d and Cyp2c knockout mice and human liver microsomes; n=2 for the hPXR/CAR/CYP3A4/7/2D6/2C9 and Cyp2c/Cyp2d/Cyp3a knockout mice).

Figure 4 Inhibition of midazolam 1'-hydroxylation by CYP3cide in a range of liver microsomal samples. Formation of 1'-hydroxymidazolam was measured in pooled liver microsomes from WT (n=3), Cyp2c knockout (n=2), Cyp3a knockout (n=2) and RIF-treated hPXR/CAR/CYP3A4/7 (n=2) and hPXR/CAR/CYP3A4/7/2D6/2C9 mice (n=2), as well as by recombinant CYP3A4 co-expressed with cytochrome P450 reductase in bacterial membranes (rCYP3A4). Data are presented as mean ± SD (n=3 measurements for each microsomal sample).

Figure 5 Whole blood concentration versus time profiles of midazolam and ketoconazole in hPXR/CAR/CYP3A4/7/2D6/2C9 mice. (**a**) MDZ concentration versus time dependencies in hPXR/CAR/CYP3A4/7/2D6/2C9 mice treated with vehicle, RIF only or RIF and KTZ. (**b**)

MDZ area under the concentration versus time curve ($AUC_{0\text{-}1440min}$). (**c**) KTZ pharmacokinetics in hPXR/CAR/CYP3A4/7/2D6/2C9 mice. All data are expressed as mean ± SD (n=3 mice per treatment group)

DMD Fast Forward. Published on August 11, 2015 as DOI: 10.1124/dmd.115.065656
This article has not been copyedited and formatted. The final version may differ from this version.

Tables

TABLE 1

Kinetic parameters of midazolam 1'-hydroxylation inhibition by erythromycin in liver microsomes of different origin.

Microsomes origin	IC_{50} (μM) ±SE	K_I (μM) ±SE	k_{inact} (min^{-1}) ±SE	k_{inact}/K_I ($mM^{-1}*min^{-1}$)
WT	1750±595	960±227	0.04±0.022	0.0417
HLM	93±16	45±7	0.03±0.013	0.67
hPXR/CAR/CYP3A4/7/2D6/2C9	220±54	137±30	0.12±.034	0.88

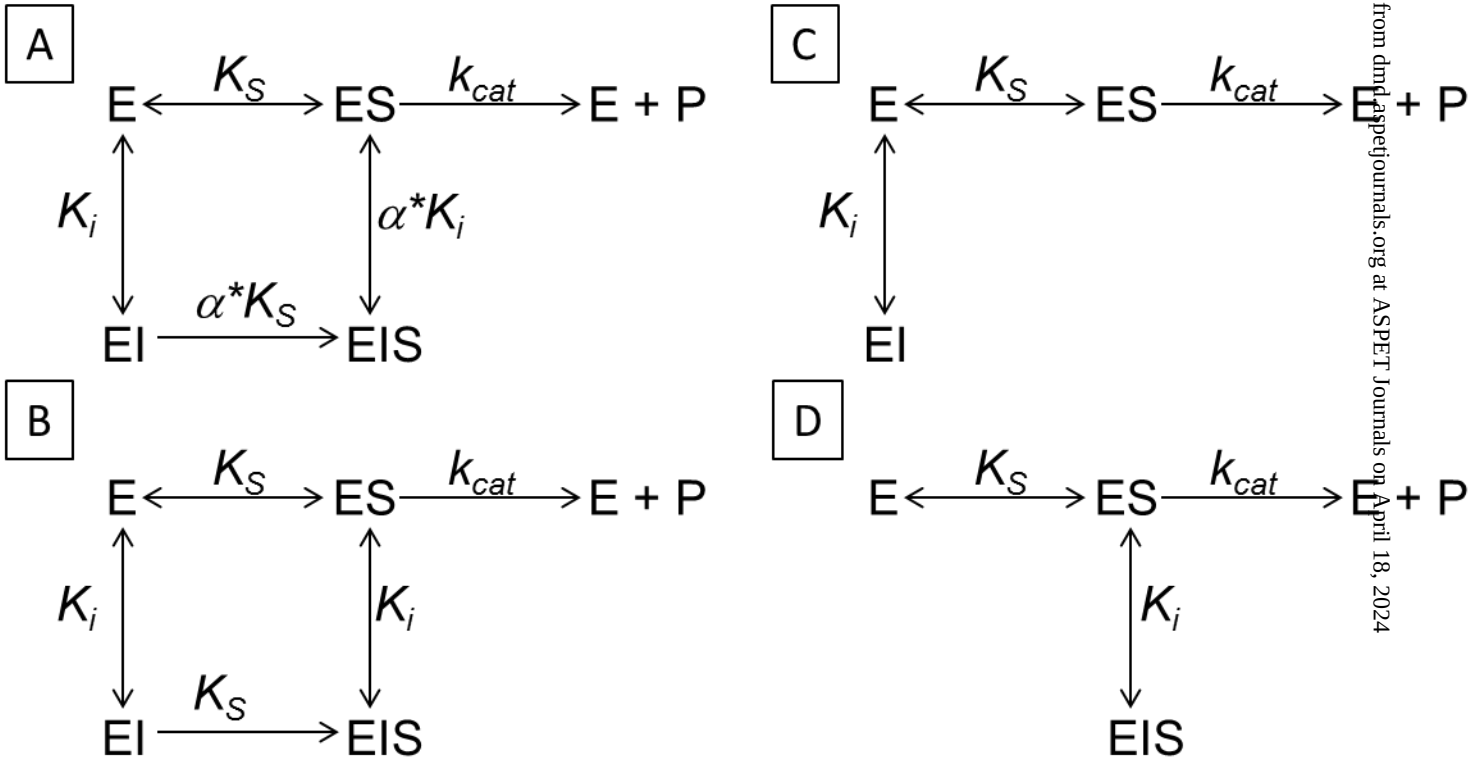

Scheme 1

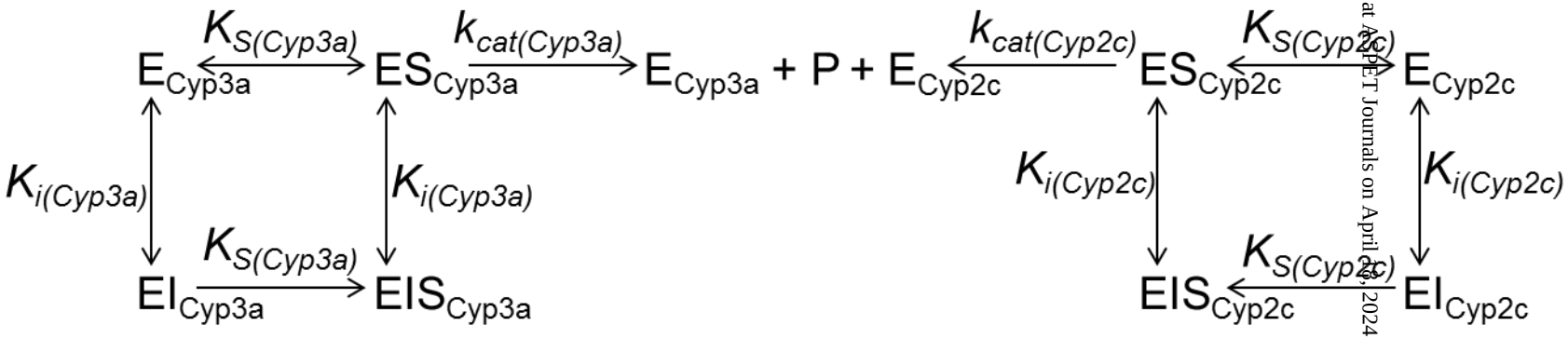

Scheme 2

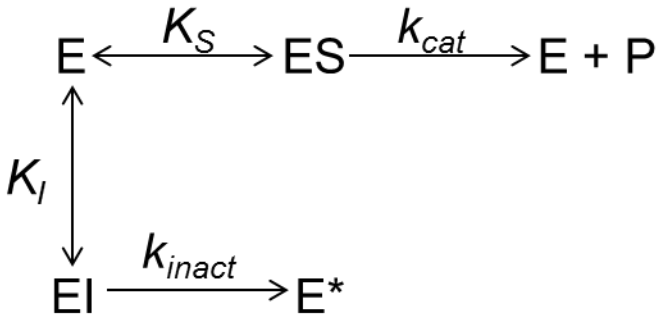

Scheme 3

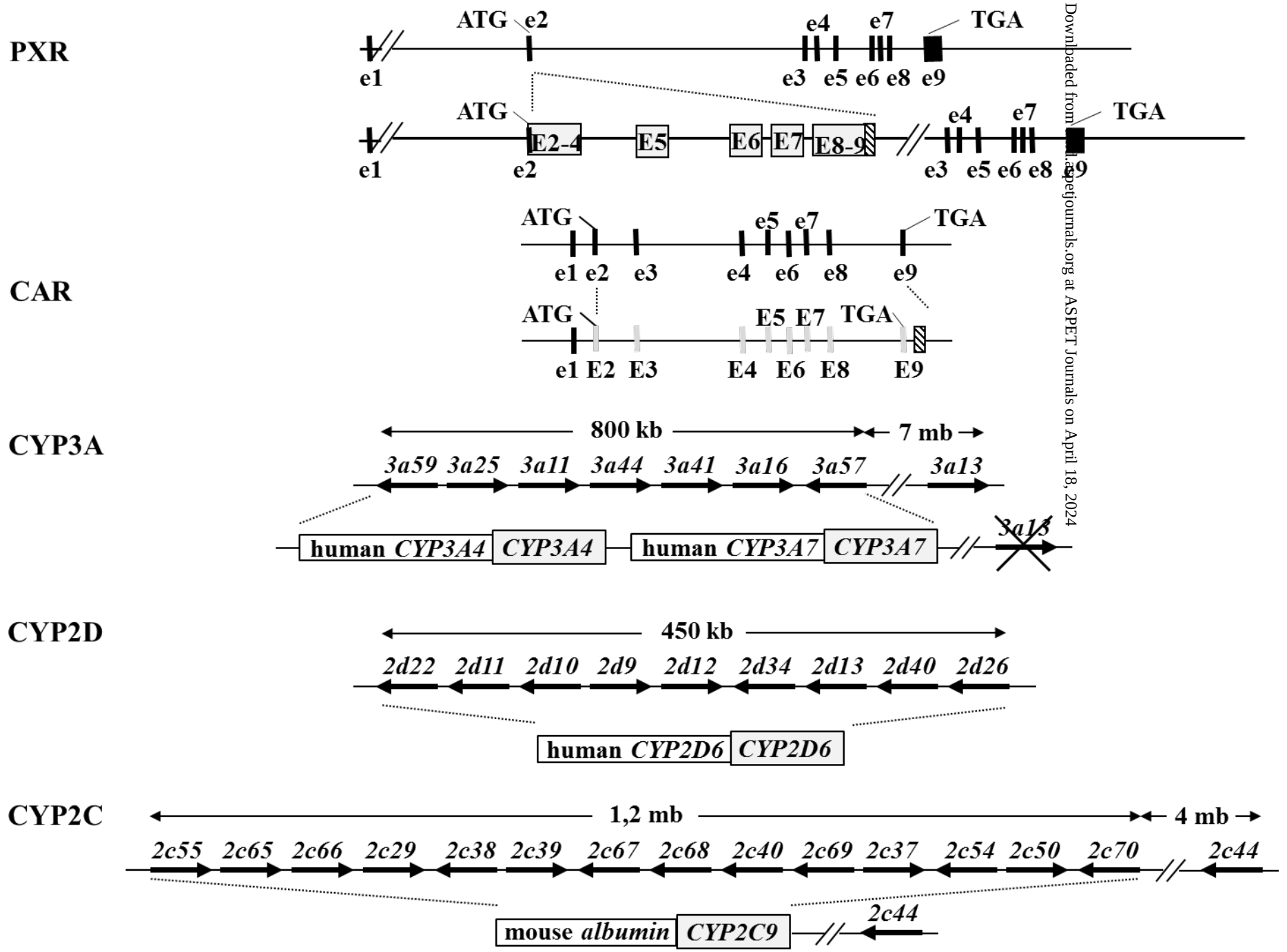

Figure 1

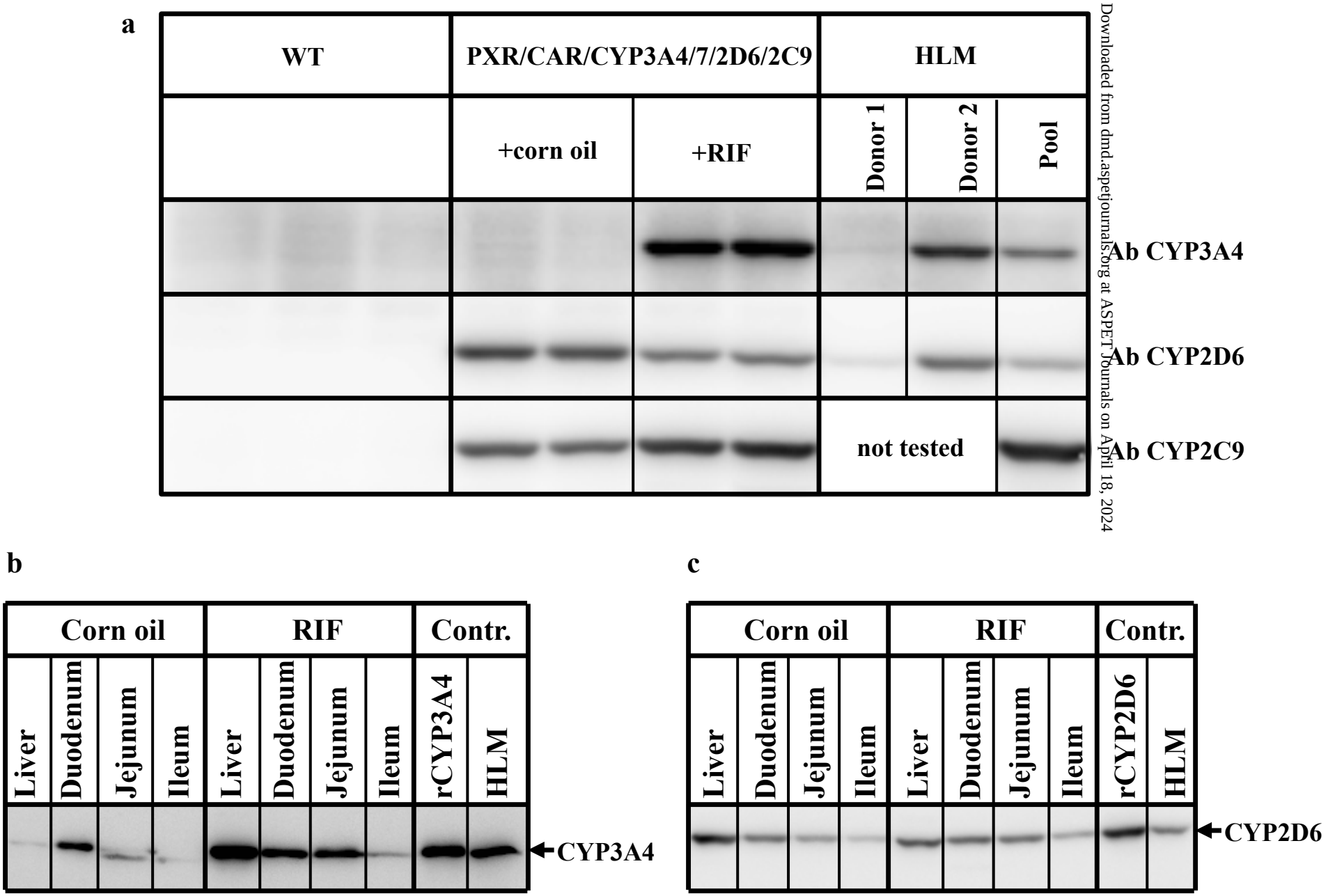

Figure 2

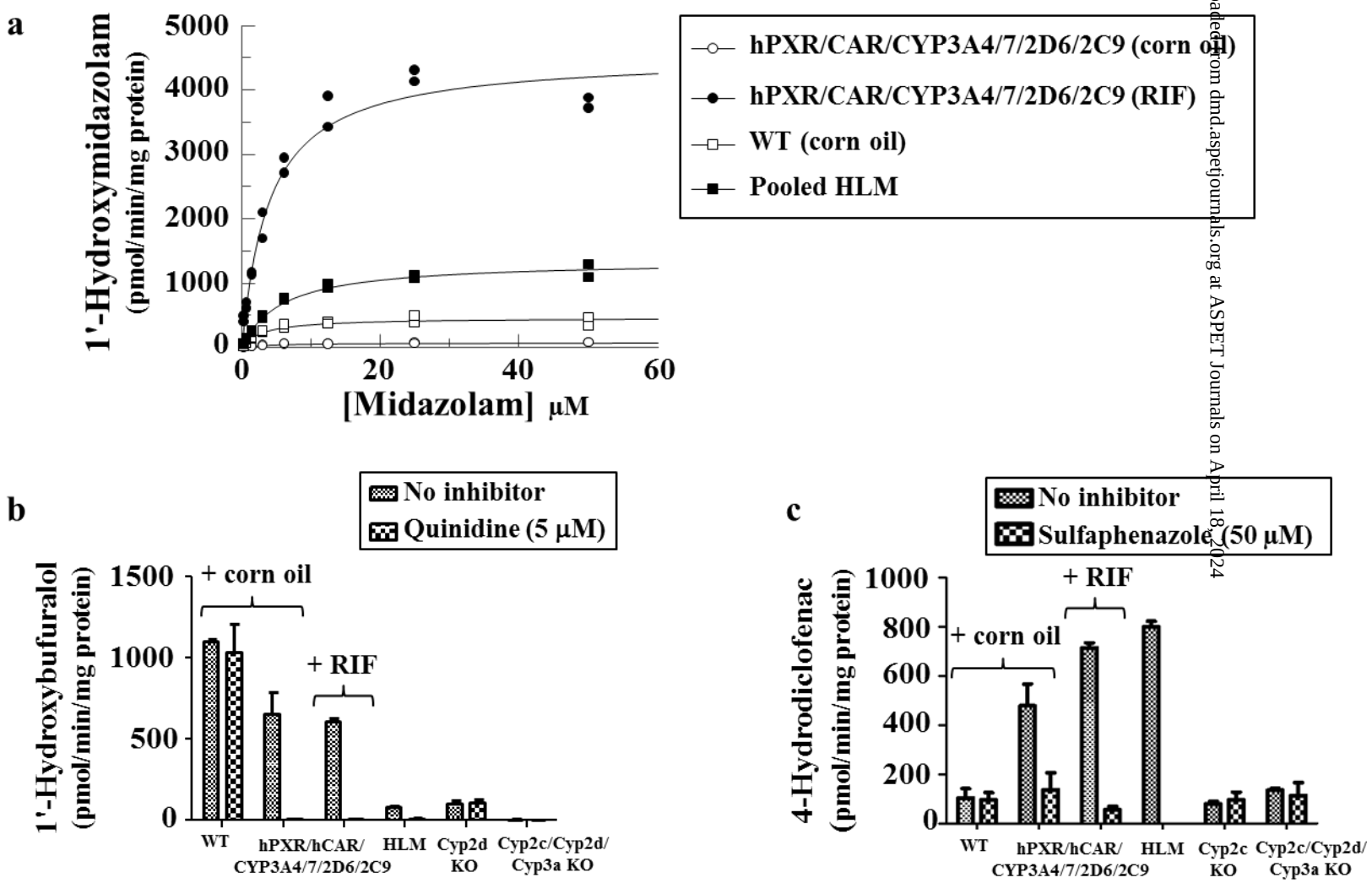

Figure 3

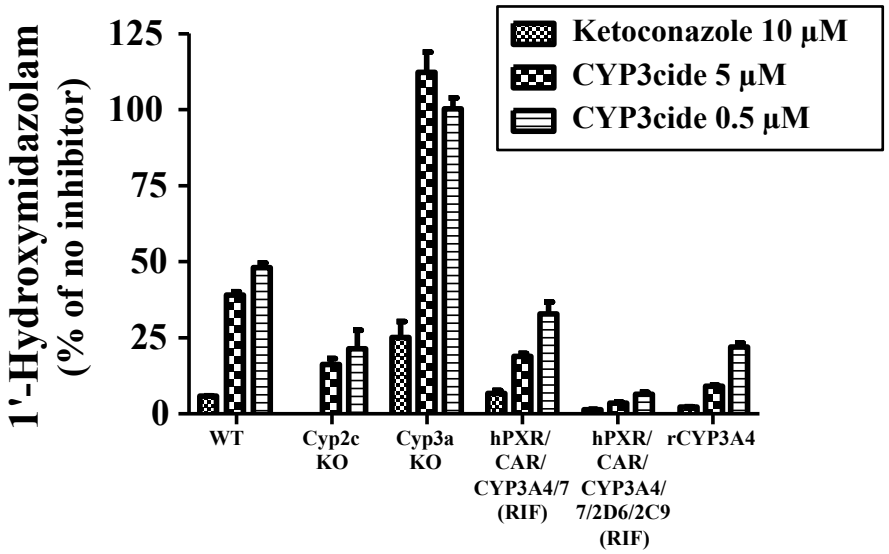

Figure 4

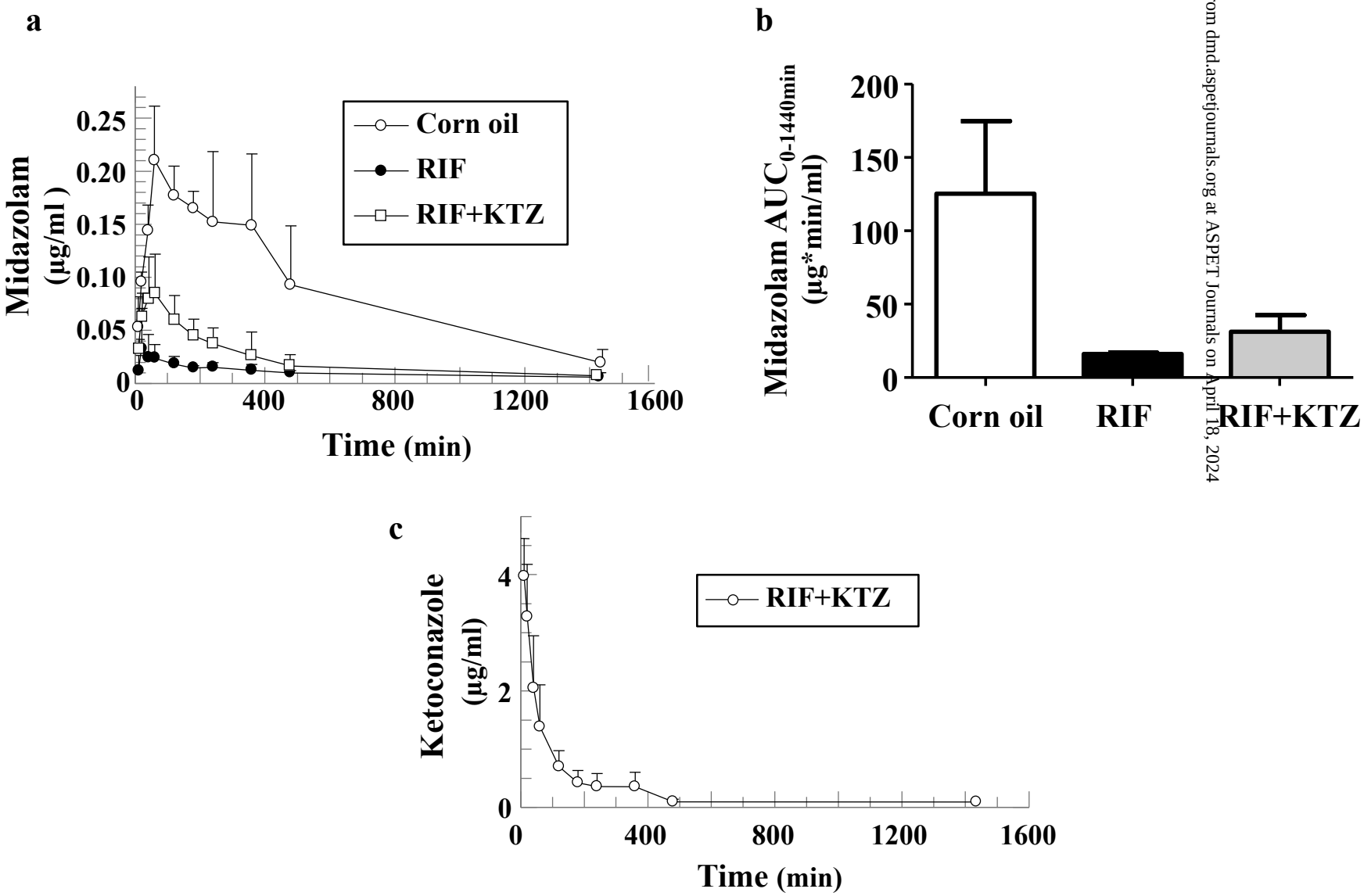

Figure 5